APPLICATIONS OF SLIDING MODE CONTROLLER AND LINEAR ACTIVE DISTURBANCE REJECTION CONTROLLER TO A PMSM SPEED SYSTEM

YANG ZHAO

Bachelor of Electrical Engineering

Shenyang University of Technology

July, 2009

Submitted in partial fulfillment of requirements for the degree

MASTER OF SCIENCE IN ELECTRICAL ENGINEERING

at the

CLEVELAND STATE UNIVERSITY

August, 2013

This thesis has been approved
for the Department of Electrical and Computer Engineering
and the College of Graduate Studies by

_____

Thesis Committee Chairperson, Dr. Lili Dong

_____

Department/Date

_____

Committee Member, Dr. Eugenio Villaseca

_____

Department/Date

_____

Committee Member, Dr. Siu-Tung Yau

_____

Department/Date

ACKNOWLEDGEMENTS

I would like to thank my advisor Dr. Lili Dong, who offered me the great opportunity to do research with her during the past three years. Dr. Lili Dong's profound thinking to engineering problems and her strict attitude to research helped me construct a systematic concept of analyzing and solving engineering problems.

I also would like to thank the committee members Dr. Villaseca and Dr. Yau for reviewing my thesis and offering constructive advices.

I would like to thank Dr. Zhiqiang Gao for his valuable suggestions and concerning for my research work. Dr. Zhiqiang Gao's explicit explanation of advanced control technologies broaden my horizon.

I would like to thank Dr. Sally Shao for her consideration and valuable suggestions for my research work.

I would like to thank my peers Shen Zhao, Qinling Zheng, Xiao Wang, Chintan Trivedi, Han Zhang and Xin Hui for sharing their ideas with me, which helped me with my research work.

I would like to thank my parents for their support and concerning, which encouraged and strengthened me to accomplish this program.

APPLICATIONS OF SLIDING MODE CONTROLLER AND LINEAR ACTIVE DISTURBANCE REJECTION CONTROLLER TO A PMSM SPEED SYSTEM

YANG ZHAO

ABSTRACT

Permanent magnet synchronous motor (PMSM) is a popular electric machine in industry for its small volume, high electromagnetic torque, high reliability and low cost. It is broadly used in automobiles and aircrafts. However, PMSM has its inherent problems of nonlinearity and coupling, which are challenges for control systems design. In addition, the external disturbances such as load variation and noises could degrade the system's performance. Both sliding mode control (SMC) and active disturbance rejection control (ADRC) are robust against disturbances. They can also compensate the nonlinearity and couplings of the PMSM. Therefore, in this thesis, we apply both SMC and ADRC to a PMSM speed system. Our control goal is to drive the speed outputs of the PMSM speed system to reference signals in the presences of nonlinearity, disturbance, and parameter variations. Simulation results verify the effectiveness of SMC and ADRC on the speed control for PMSM systems in spite of the presences of external disturbance and internal system uncertainties.

TABLE OF CONTENTS

Page

LIST OF TABLES

LIST OF FIGURES

NOMENCLATURE

PM: Permanent magnet

DC: Direct current

AC: Alternate current

BLDCM: Brushless direct current motor

PMSM: Permanent magnet synchronous motor

Back-EMF: Back electromotive force

PI: Proportional integral

PD: Proportional derivative

PID: Proportional integral derivative

FOC: Field oriented control

DTC: Direct torque control

FLC: Fuzzy logic control

VSC: Variable structure control

SMC: Sliding mode control

ADRC: Active disturbance rejection control

LADRC: Linear active disturbance rejection control

ESO: Extended state observer

LESO: Linear extended state observer

KVL: Kirchhoff’s voltage laws

CHAPTER I

INTRODUCTION

1.1 Background

Electric motors play an important role in modern world because most of the physical motions in machines such as hand power tools, air compressors and water pumps, etc. are driven by electric motors. Among all types of motors, permanent magnet (PM) motors became increasingly popular and they have been widely used in automobiles, aircrafts and industrial machines [1-3].

PM motors do not need commutator or brush compared to direct current (DC) motors. Thus they have simpler structure, better reliability and lower maintenance cost [2].

In addition, PM motors do not need exciting currents for the magnetic field in its air gap compared to induction motors. Therefore PM motors have lower power consumption on armature windings, higher efficiency and simpler controller [2].

In general, PM motors have the advantages of small volume, low noise, high power density, high electromagnetic torque, high efficiency, high dynamic performance and low cost [1-3].

PM motors can be mainly classified as brushless direct current (BLDC) motor and permanent magnet synchronous motor (PMSM) [3]. The mechanical structures of BLDC and PMSM are almost the same, except that the designs of the permanent magnets on rotors for these two motors are different [3]. The supply currents of BLDC motor are three-phase square waves while the supply currents of PMSM are three-phase sine waves [3]. The ideal back electromotive force (back-EMF) of BLDC motor is in square wave form and the ideal back-EMF of PMSM is in sine wave form [3]. But in reality, the back-EMF of BLDC motor is usually in trapezoidal wave form due to the imperfection of the shapes of permanent magnets of BLDC motors [1], which leads to considerable torque ripples and speed oscillation in BLDC motors.

PMSM has smaller torque ripples than BLDC motor, which makes PMSM more suitable for high precision speed systems.

1.2 Literature Review

Although PMSM has the advantages listed above that attract attention from researchers and manufactures, it also has inherent problems such as nonlinearity and coupling [4]. There is not only self-inductance in each phase but also mutual-inductance between each two phases in the stator of PMSM, which resulting in coupling. PMSM can

only be controlled by three-phase stator currents since there is no excitation winding on the rotor. But the excitation magnetic field from permanent magnets on the rotor has strong nonlinear influence on the stator windings. In addition, the parameter variations such as friction variation and moment of inertia variation have considerable influence on PMSM [5-6]. Finally, the external disturbances such as load variation and noise would degrade the performance of PMSM significantly [5-7].

The coupling problem of PMSM can be solved by adopting field oriented control (FOC) strategy [8-10]. FOC was firstly introduced by F. Blaschke in 1971 to solve induction motor control problems [11]. Then, FOC was studied by many researchers and it was successfully applied to many alternate current (AC) drives in industry [11]. Nowadays, FOC is the main decoupling control method for PMSM and its decoupling function is realized by coordinate transformation [1].

The other wildly used control strategy for PMSM is direct torque control (DTC) [12-14]. DTC was firstly presented by I. Takahashi and T. Noguchi in 1986 to control induction motors [13]. DTC controls the magnetic toque and flux linkage of AC motors directly without any decoupling calculation [12]. DTC was also successfully applied on PMSM [14].

The comparison study between FOC and DTC indicates that the response of PMSM speed control to DTC is faster than FOC with more torque ripples, and the response of PMSM speed control to FOC is more precise than DTC with less torque ripples [8, 12].

PI controllers are popular for PMSM control in industry because of its simple structure, easy implementation and reliability [5, 6, 15, 16]. However, PI controllers are

not robust enough against plant parameter variations and external disturbances [5, 6, 15-18]. When there is nonlinear parameter variations in PMSM, the operating point of PMSM changes accordingly, so that linear PI controllers with fixed controller gains need to be tuned again or the performance of PMSM control system will be degraded [16, 19]. But PI controllers are still a good choice for PMSM control system if the high precision performance of PMSM is not demanded.

Fuzzy logic control (FLC) overcomes the limitation of linear PI controller since the FLC's controller gains can be decided online according to the error signal and changing tendency of error signal [20-25]. FLC is robust against the nonlinearity of PMSM and sudden load variation of PMSM control system [20-25]. But the design process and tuning of FLC is complicated, so that it is laborious and time consuming to design a proper FLC for PMSM control systems in practice.

Adaptive control was successfully applied to PMSM control systems for its insensitivity to system uncertainties [26-31]. The unknown parameters of PMSM are estimated by adaptive laws online. The adaptive control signal that is based on the estimated parameters can compensate the parameter variations and load variations [26-31]. Adaptive control is an effective solution to solve specific PMSM control problems that are caused by certain parameters such as the torque ripples [27-29]. The performance of adaptive control is dependent on mathematical modeling of the PMSM system. It would be degraded in practice since an accurate mathematical model is hard to obtain.

Variable structure control (VSC) was first proposed by Soviet researchers Emelyanov and Utkin in the 1950s [32, 33]. From 1950s to 1960s, VSC was studied to solve the control problems of second-order linear systems [32, 33]. From 1960s to 1970s,

VSC was further studied to solve the control problems of higher order linear systems [33]. VSC and SMC were first published in English by Utkin in 1977 [34], and then VSC and SMC were studied and applied to solve many control problems [32, 33]. SMC is a robust control method that is insensitive to systems uncertainties, parameter variations and external disturbances [32]. And many SMC control methods have been applied to PMSM [35-44]. The major drawback of the classical SMC is its chattering problem [32, 45]. So some complex algorithms such FLC and adaptive control are combined with SMC to solve this problem [37, 40], which makes the SMC lose the advantage of simplicity. Nowadays the main SMC research topics for PMSM include sliding mode observer [35] and chattering free control [36].

ADRC was first proposed by J. Q. Han in Chinese in 1998 [46]. The original ADRC consists of a nonlinear tracking-differentiator [47], a nonlinear state error feedback controller [48] and an extended state observer (ESO) [49]. ADRC was first published in English in 2001 [50]. And the concepts of linear extended state observer (LESO) and linear active disturbance rejection control (LADRC) were proposed by Z. Q. Gao in 2003 [51], who simplified the design process of ADRC. Han's ADRC is insensitive to system uncertainties and external disturbances [46], and it was successfully applied to PMSM control system [4, 5, 15, 52, 53]. But Han's ADRC is relatively complex for control design and tuning while LADRC is easier for design and implementation in the real world.

1.3 Thesis Contribution

Both a pure SMC and a LADRC are originally developed for a PMSM speed system. They are implemented on a PMSM speed system using Matlab/Simulink to drive the speed outputs to the references. The comparison study between these two advanced control methods from the aspects of dynamic performance, and their robustness against disturbances and parameter variations is presented. The simulation results demonstrated the effectiveness of the two controllers.

1.4 Outline

The rest of the thesis is organized as follows. The dynamic modeling of a PMSM speed system is introduced in Chapter II. A SMC is developed on the PMSM speed system in Chapter III. A LADRC is developed on the PMSM speed system in Chapter IV. The simulation results for both SMC and LADRC on the PMSM speed system are presented in Chapter V. The concluding remarks and future research are provided in Chapter VI.

CHAPTER II

PMSM SPEED SYSTEM

2.1 Introduction

PMSM speed systems refer to the systems that take the speed of PMSM as the major control object with speed sensors or sensorless calculation.

PMSM speed systems are designed to satisfy specific industrial manufacture processes or customer requirements. A high performance PMSM speed system requires fast and smooth transient response without overshoot, a stable steady state response without error and robustness against disturbances and parameter variations.

There are speed feedback control loop and current feedback control loops in PMSM speed systems. The current controllers are used to control the electromagnetic torque and flux linkage in PMSM. The speed controller is used to drive the speed outputs to the speed references. The output of the speed controller is the input of current control loop and the performance of speed controller affects the overall performance of the system. So the design of speed controller is critical for PMSM speed systems.

The block diagram of PMSM speed system is presented in Figure 2.1. The currents converter is used to converter three-phase currents to two-phase currents.

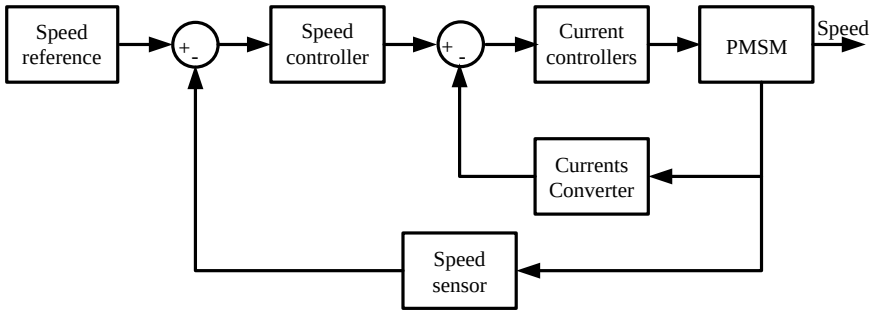

Figure 2.1: Block diagram of PMSM speed system

2.2 Permanent Magnet Synchronous Motor

2.2.1 Mechanical Structure

PMSM is an AC electric machine whose rotor is mounted with permanent magnets instead of windings.

PMSM is constructed with stator and rotor [1-3]. The air gap magnetic field of PMSM is mainly provided by permanent materials on the rotor and the stator magnetic field is generated by three-phase sinusoidal currents [3]. A schematic diagram of PMSM's mechanical structure is presented in Figure 2.2.

In Figure 2.2, the stator, iron core and shaft are made of silicon steel, and the slots in the stator are used for placing windings [1-3]. The permanent materials could be alnicos (*Al, Ni, Co, Fe*), Ceramics (barium ferrite $BaO \times 6Fe_2O^3$, strontium ferrite

$SrO \times 6Fe_2O^3$) or rare-earth materials (samarium-cobalt *SmCo*, neodymium-iron-boron *NdFeB*) [3]. The permanent materials are firmly installed on the rotor and *N* represents the North Pole and *S* represents the South Pole.

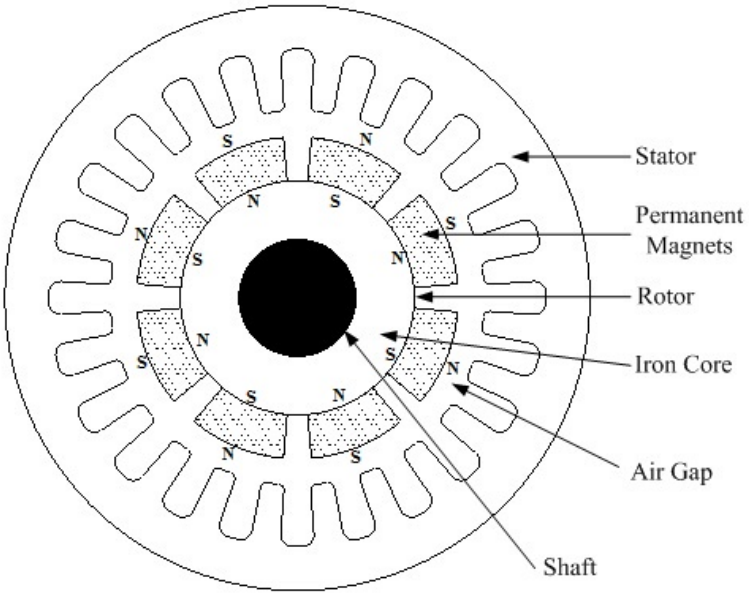

Figure 2.2: Mechanical structure of PMSM [1]

2.2.2 Rotating Magnetic Field

The PMSM stator is winded with copper wires that are distributed to three-phases. When three-phase sinusoidal currents are applied to the windings, a rotating magnetic field is generated, which drives the rotor to rotate with it at synchronous speed.

There are two major stator winding connection patterns: distributed windings and concentrated windings. Distributed winding has the advantage of even magnetic field

distribution in sinusoidal form, but it requires more coils that take more space [54]. And concentrated winding has the advantages of less cost of coils and small volume, but its magnetic field is not as evenly distributed as distributed winding [54].

We take one-pole-pair PMSM for an example to explain how stator windings generate rotating magnetic field. The windings are usually star-connected as shown in Figure 2.3. In this figure, u_A, u_B and u_C represent three-phase supply voltages and i_A, i_B and i_C represent three-phase supply currents. *A*, *B* and *C* represent the input ports of each phase and *X*, *Y* and *Z* represent the terminal ports of each phase. Since the three-phase windings are star-connected, *X*, *Y* and *Z* are connected at the same point.

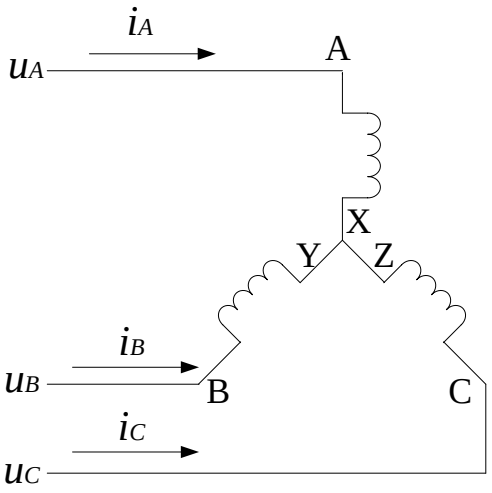

Figure 2.3: Two pole pair PMSM Y-connection stator windings [55]

There is a 120^o phase difference between each two of the three-phase currents as shown in (2.1) and Figure 2.4.

$$\begin{cases} i_A = I_m sin\omega_e t \\ i_B = I_m \sin\left(\omega_e t - \dfrac{2\pi}{3}\right) \\ i_C = I_m \sin\left(\omega_e t - \dfrac{4\pi}{3}\right) \end{cases} \tag{2.1}$$

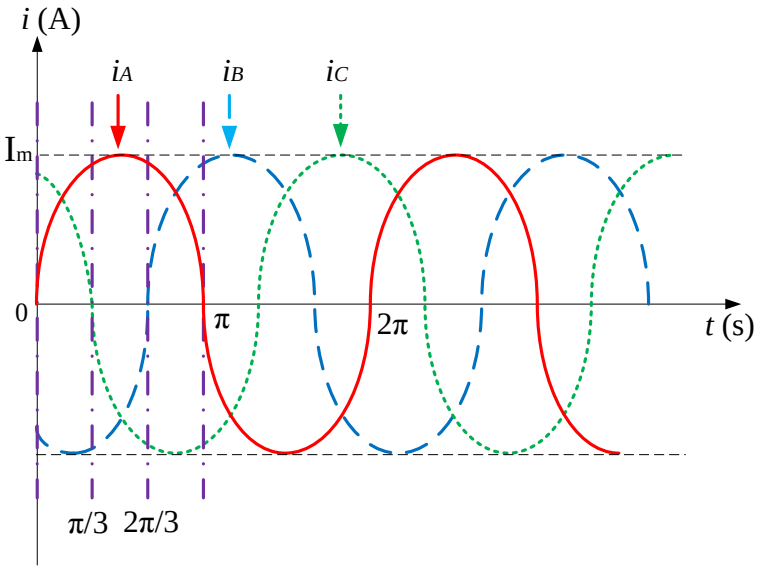

Figure 2.4: Three-phase sinusoidal supply currents

In (2.1) and Figure 2.5, i_A, i_B and i_C represent the instant currents in the three-phases. Parameter I_m represents the current peak value. Parameter ω_e represents the angular electrical frequency and *t* represents time.

Since the supply currents are consistent, the rotating magnetic field is continuous. In order to illustrate the relationship of rotating magnetic field positions and supply currents, four specific moments are taken: $t_1 = 0(s)$, $t_2 = \frac{\pi}{3}(s)$, $t_3 = \frac{2\pi}{3}(s)$ and $t_4 = \pi(s)$.

The corresponding rotating magnetic field positions of distributed windings are shown in Figure 2.5, Figure 2.6, Figure 2.7, and Figure 2.8. Define the anticlockwise direction is positive and phase *A* as zero degree. The direction of magnetic field is decided by Ampere's circuital law, and *N* represents the North Pole and *S* represents the South Pole. The parameter ω_e represents electrical angular speed and $\omega_e t$ represents the electrical angular position. When the current value is positive, the current is feeding in the winding, so a cross symbol is used. When the current is flowing out of an end, a dot symbol is used.

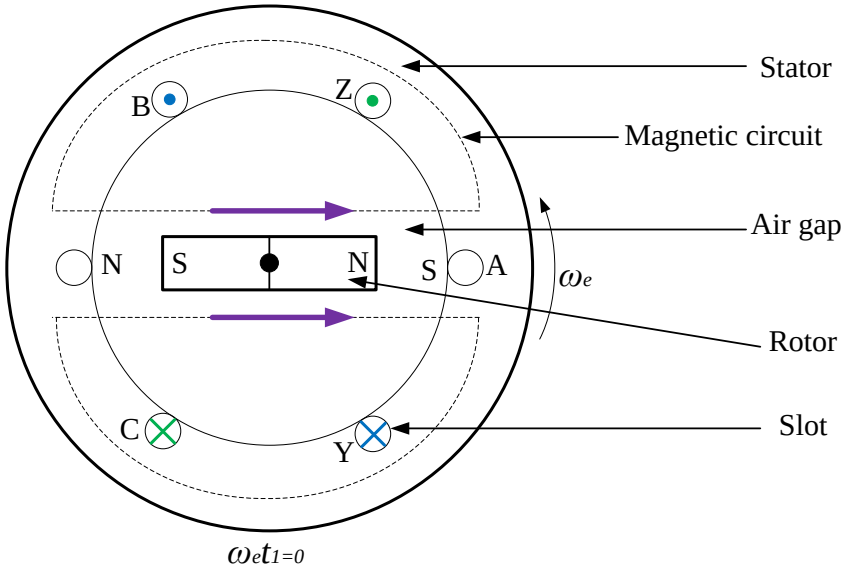

Figure 2.5: Rotating magnetic field of distributed windings at $\omega_e t_1 = 0$

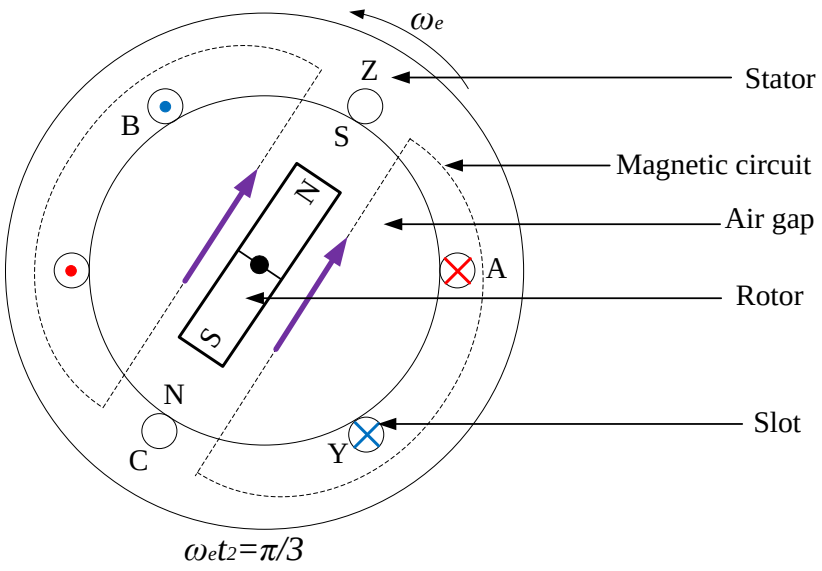

Figure 2.6: Rotating magnetic field of distributed windings at $\omega_e t_2 = \pi / 3$

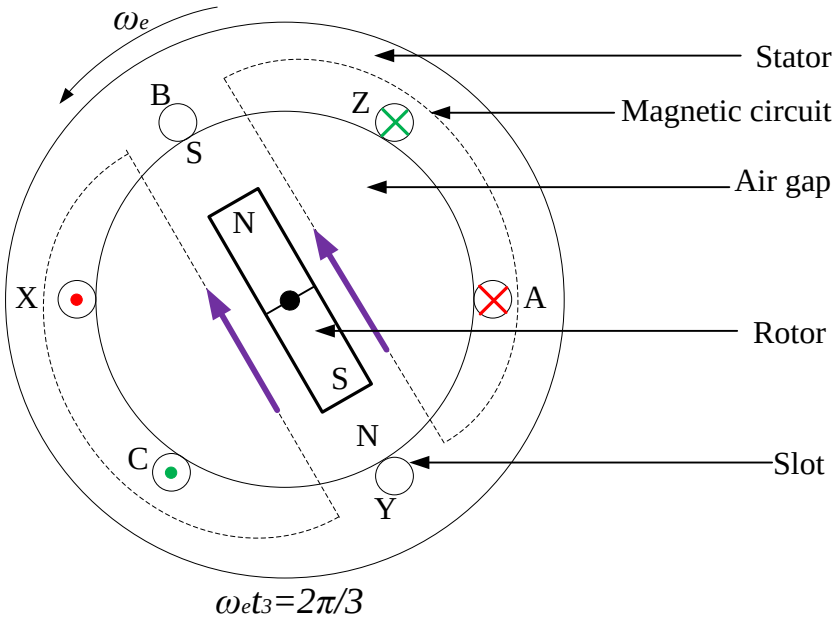

Figure 2.7: Rotating magnetic field of distributed windings at $\omega_e t_3 = 2\pi / 3$

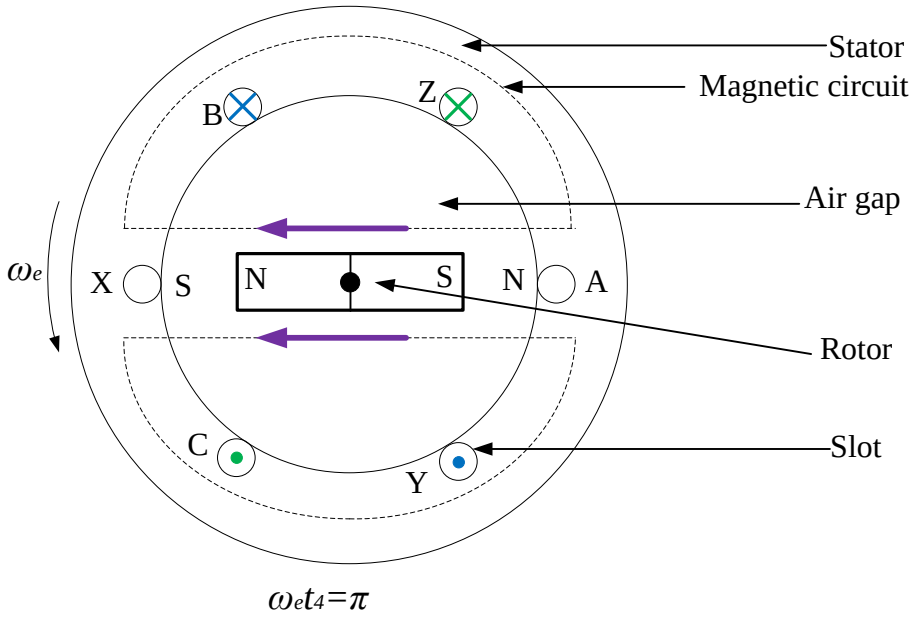

Figure 2.8: Rotating magnetic field of distributed windings at $\omega_e t_4=\pi$

From Figure 2.5 to Figure 2.8, the magnetic circuit includes stator and the air gap. The stator silicon steel will generate some small currents in the changing magnetic field, resulting in producing heat. This phenomenon is defined as eddy current loss [1-3]. Also the flux changing rate of the stator silicon steel is slower than the flux changing rate generated by supply currents, resulting in the stator silicon steel absorbing small amount energy from the magnetic field to maintain the same flux value. This phenomenon is defined as hysteresis loss [1-3]. The magnetic flux capacity of the stator silicon steel is limited, so the flux cannot be increased at its limitation value. This phenomenon is defined as magnetic saturation [1-3].

When the rotor rotates, a voltage is generated by the rotor flux in the stator windings and this voltage is opposite to the supply voltage. This voltage is defined as back-EMF.

2.3 Coordinate Transformations

Coordinate transformation is used for FOC realization and PMSM mathematical model simplification, so the understanding of coordinate transformation is necessary for the control of PMSM.

Three coordinates are defined and they are the *A*-*B*-*C* stationary coordinate, the α-β stationary coordinate and the *d*-*q* rotating coordinate.

Figure 2.9 shows the *A*-*B*-*C* stationary coordinate. In Figure 2.9, there is 120º phase difference between each two of the three phases. The three-phase currents i_A, i_B and i_C of PMSM are assigned along phase *A*, phase *B* and phase *C* respectively. Then the three-phase currents i_A, i_B and i_C are considered as three space vectors, and the three-phase currents together constitute a composite vector i_S.

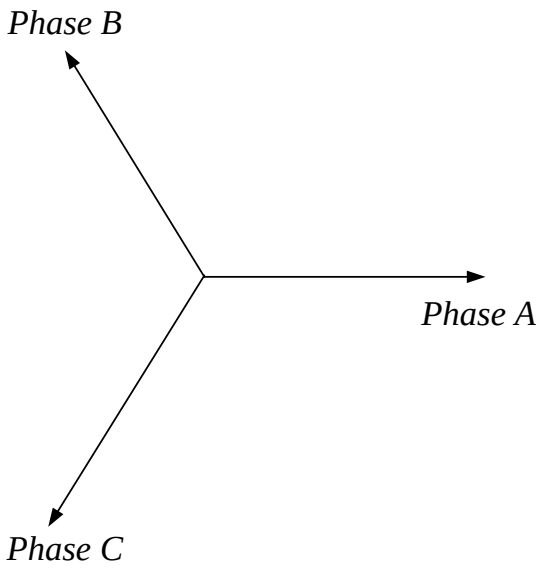

Figure 2.9: The *A*-*B*-*C* stationary coordinate

Define the anticlockwise as positive direction and phase *A* as zero degree. Suppose the composite vector i_S rotates at a constant speed ω_e in positive direction. The composite vector i_S in the *A*-*B*-*C* stationary coordinate is presented in Figure: 2.10.

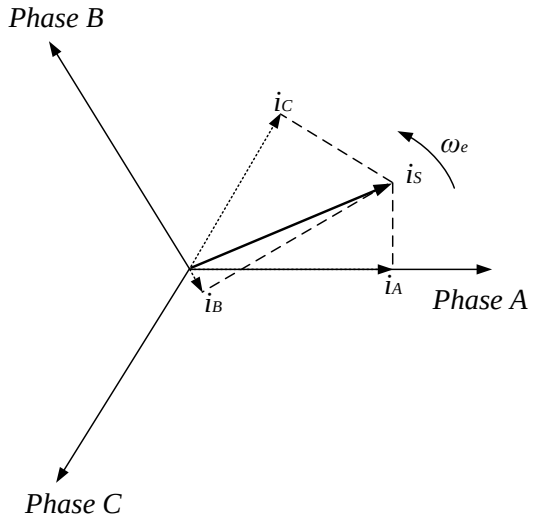

Figure 2.10: Composite vector in the *A*-*B*-*C* stationary coordinate

Figure 2.11 shows the α- β stationary coordinate. In Figure 2.11, phase α and phase β are orthogonal to each other and the current i_α and i_β are defined as the current vectors along phase α and phase β.

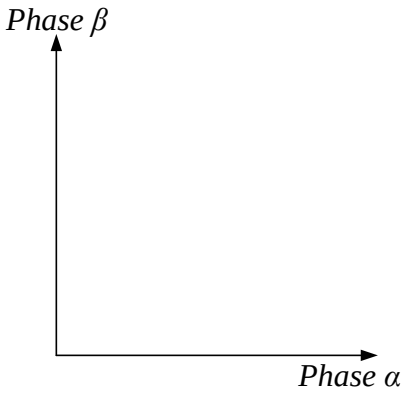

Figure 2.11: The α-β stationary coordinate

Figure 2.12 shows the α- β stationary coordinate. The composite vector i_S can be composed by these two orthogonal space vectors i_α and i_β.

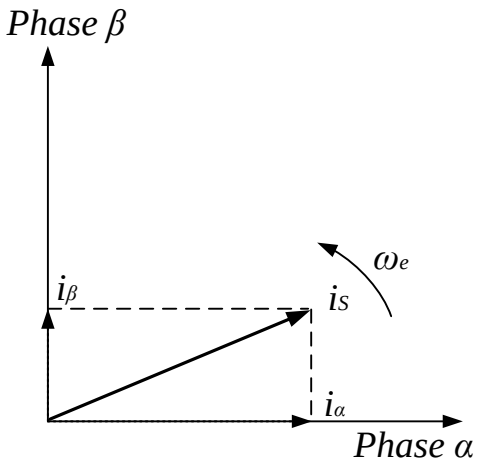

Figure 2.12: Composite vector in the α-β stationary coordinate

Figure 2.13 shows the *d*- *q* rotating coordinate. In Figure 2.13, the phase *d* and phase *q* are orthogonal to each other and the currents i_d and i_q are defined as the current vectors along phase *d* and phase *q*.

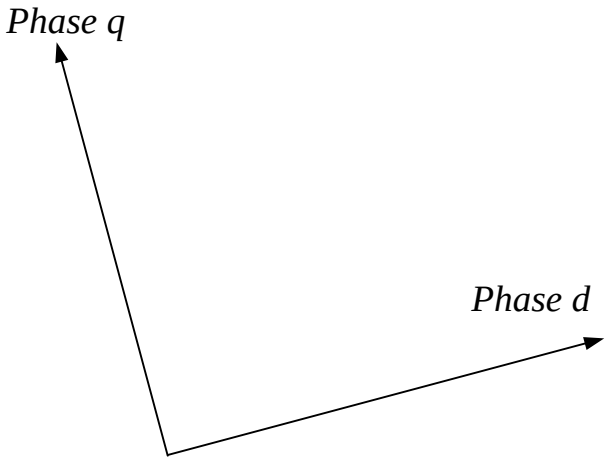

Figure 2.13: The *d*-*q* rotating coordinate

Figure 2.14 shows the composite vector i_S in the *d- q* rotating coordinate. The composite vector i_S can be composed by i_d and i_q. The amplitude of i_d and i_q remain the same, and the *d-q* rotating coordinate rotates at the constant speed ω_e. And the angle between phase *d* and phase *A* is defined as θ_e.

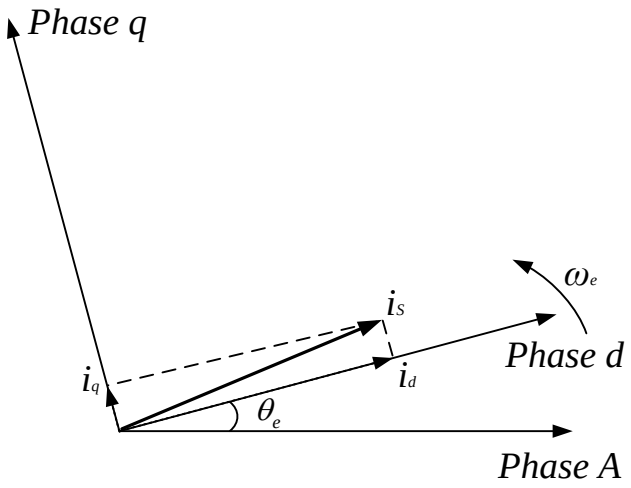

Figure 2.14: Composite vector in the *d-q* rotating coordinate

The propose of coordinate transformation is to convert the current vectors i_A, i_B and i_C to current vectors i_d and i_q. Figure 2.15 shows the relationship between PMSM rotor and the *d-q* rotating coordinate. In Figure 2.15, the phase *d* is assigned along the rotor flux of PMSM and ω_e represents the angular electrical speed and θ_e represents the angular electrical position.

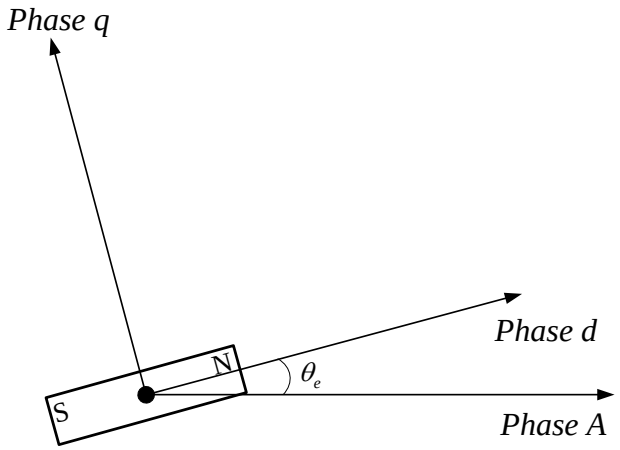

Figure 2.15: Relationship between PMSM rotor and *d-q* rotating coordinate

The transformation from current vectors i_A, i_B and i_C to current vectors i_α and i_β is defined as Clarke transformation. And the transformation from current vectors i_α and i_β to current vectors i_A, i_B and i_C is defined as Inverse Clarke transformation.

The Clarke transformation can be represented by:

$$\begin{bmatrix} i_\alpha \\ i_\beta \end{bmatrix} = \sqrt{\frac{2}{3}} \begin{bmatrix} 1 & -\frac{1}{2} & -\frac{1}{2} \\ 0 & \frac{\sqrt{3}}{2} & -\frac{\sqrt{3}}{2} \end{bmatrix} \begin{bmatrix} i_A \\ i_B \\ i_C \end{bmatrix} \tag{2.2}$$

The Inverse Clarke transformation can be represented by:

$$\begin{bmatrix} i_A \\ i_B \\ i_C \end{bmatrix} = \sqrt{\frac{2}{3}} \begin{bmatrix} 1 & 0 \\ -\frac{1}{2} & \frac{\sqrt{3}}{2} \\ -\frac{1}{2} & -\frac{\sqrt{3}}{2} \end{bmatrix} \begin{bmatrix} i_\alpha \\ i_\beta \end{bmatrix} \tag{2.3}$$

The transformation from current vectors i_α and i_β to current vectors i_d and i_q is defined as Park transformation. And the transformation from current vectors i_d and i_q to current vectors i_α and i_β is defined as Inverse Park transformation.

The Park transformation can be represented by:

$$\begin{bmatrix} i_d \\ i_q \end{bmatrix} = \begin{bmatrix} \cos\theta_e & \sin\theta_e \\ -\sin\theta_e & \cos\theta_e \end{bmatrix} \begin{bmatrix} i_\alpha \\ i_\beta \end{bmatrix} \tag{2.4}$$

The Inverse Park transformation can be represented by:

$$\begin{bmatrix} i_\alpha \\ i_\beta \end{bmatrix} = \begin{bmatrix} \cos\theta_e & -\sin\theta_e \\ \sin\theta_e & \cos\theta_e \end{bmatrix} \begin{bmatrix} i_d \\ i_q \end{bmatrix} \tag{2.5}$$

In (2.4) and (2.5), θ_e represents the angular electrical position.

Combining Clarke transformation and Park transformation, we will have the transformation from current vectors i_A, i_B and i_C to current vectors i_d and i_q which is presented by (2.6). And the transformation from current vectors i_d and i_q to current vectors i_A, i_B and i_C is presented in (2.7). Again in these two equations, θ_e represents the rotor angular electrical position.

$$\begin{bmatrix} i_d \\ i_q \end{bmatrix} = \sqrt{\frac{2}{3}} \begin{bmatrix} \cos\theta_e & \cos(\theta_e - \frac{2\pi}{3}) & \cos(\theta_e + \frac{2\pi}{3}) \\ -\sin\theta_e & -\sin(\theta_e - \frac{2\pi}{3}) & -\sin(\theta_e + \frac{2\pi}{3}) \end{bmatrix} \begin{bmatrix} i_A \\ i_B \\ i_C \end{bmatrix} \tag{2.6}$$

$$\begin{bmatrix} i_A \\ i_B \\ i_C \end{bmatrix} = \begin{bmatrix} \cos\theta_e & -\sin\theta_e \\ \cos(\theta_e - \frac{2\pi}{3}) & -\sin(\theta_e - \frac{2\pi}{3}) \\ \cos(\theta_e + \frac{2\pi}{3}) & -\sin(\theta_e + \frac{2\pi}{3}) \end{bmatrix} \begin{bmatrix} i_d \\ i_q \end{bmatrix} \tag{2.7}$$

2.4 Equivalent Circuit and Mathematical Models for PMSM Systems

2.4.1 Equivalent Circuit Model in *A*-*B*-*C* Coordinate

The equivalent circuit for PMSM systems in the *A*-*B*-*C* coordinate is presented in Figure 2.16. In Figure 2.16, u_A, u_B and u_C represent the three-phase supply voltages, i_A, i_B and i_C represent the three-phase supply currents, R_S is the stator resistance in each phase, L is the stator self-inductance in each phase, M is the stator mutual-inductance between two phases, and e_A, e_B and e_C are back-EMF from the rotor side.

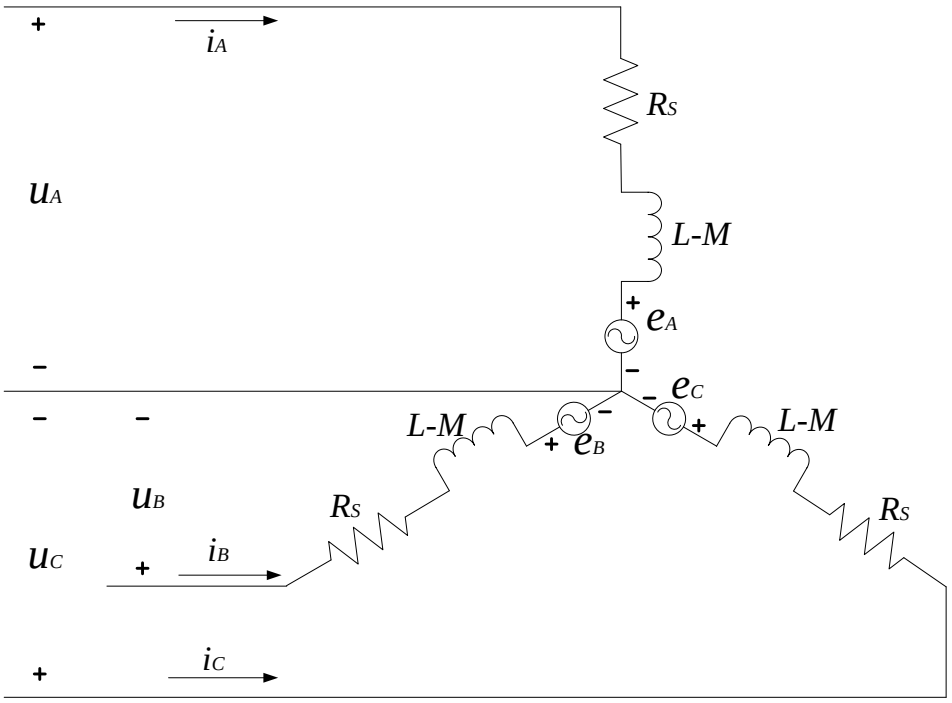

Figure 2.16: An equivalent circuit for PMSM system in A-B-C coordinates [56]

From Figure 2.16, the PMSM model in the *A-B-C* coordinate can be constructed using Kirchhoff's voltage laws (KVL).

From KVL, the voltage equations of PMSM of each phase are presented in (2.8).

$$\begin{cases} u_A = i_A R_S + (L-M)\dfrac{di_A}{dt} + e_A \\ u_B = i_B R_S + (L-M)\dfrac{di_B}{dt} + e_B \\ u_C = i_C R_S + (L-M)\dfrac{di_C}{dt} + e_C \end{cases} \tag{2.8}$$

According to the Faraday's law, the back-EMF is the derivative of rotor flux linkage.

The back-EMF equations of each phase are presented in (2.9), where ψ_f represents the rotor flux linkage and θ_e is rotor electrical angular position.

$$\begin{cases} e_A = \cos\theta_e \dfrac{d\psi_f}{dt} \\ e_B = \cos\left(\theta_e - \dfrac{2\pi}{3}\right)\dfrac{d\psi_f}{dt} \\ e_C = \cos\left(\theta_e - \dfrac{4\pi}{3}\right)\dfrac{d\psi_f}{dt} \end{cases} \tag{2.9}$$

The total flux in each phase is the combination of the stator flux and the rotor flux.

The flux equations of each phase are presented in (2.10). In (2.10), ψ_A, ψ_B and ψ_C represent the total flux in each phase.

$$\begin{cases} \psi_A = i_A(L-M) + \psi_f cos\theta_e \\ \psi_B = i_B(L-M) + \psi_f \cos\left(\theta_e - \dfrac{2\pi}{3}\right) \\ \psi_C = i_C(L-M) + \psi_f \cos\left(\theta_e - \dfrac{4\pi}{3}\right) \end{cases} \tag{2.10}$$

The electromagnetic torque equation is presented in equation (2.11). In (2.11), T_e represents electromagnetic torque and ω_e represents angular electrical speed.

$$T_e = \frac{e_A i_A + e_B i_B + e_C i_C}{\omega_e} \tag{2.11}$$

2.4.2 PMSM Equivalent Circuits and Models in the *d-q* Coordinate

The equivalent circuits of *d-q* coordinate are transformed from equivalent circuits of *A-B-C* coordinate. The details about the circuit transformation are introduced in [57]. The equivalent circuits of *d-q* coordinate are presented in Figure 2.17 and Figure 2.18. In

Figure 2.17 and Figure 2.18, R_S is the stator resistance, u_d and u_q are supply voltages. i_d and i_q are supply currents, L_d and L_q represent the self-induction in phase *d* and phase *q*, ω_e represents the angular electrical speed, and ψ_d and ψ_q represent the flux linkage in phase *d* and phase *q*.

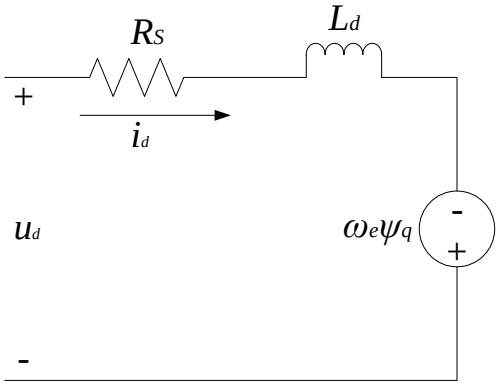

Figure 2.17: PMSM equivalent circuit in phase *d* [56]

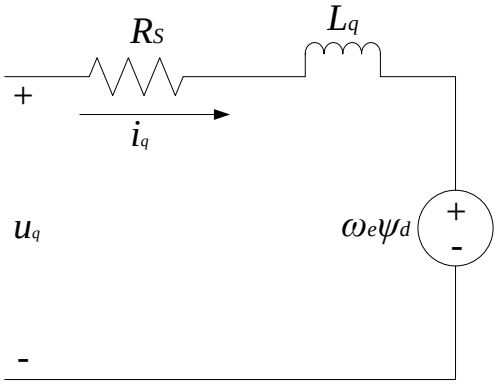

Figure 2.18: PMSM equivalent circuit in phase *q* [56]

The voltage equations in *d*-*q* coordinate are presented in (2.12).

$$\begin{cases} u_d = R_s i_d - \omega_e \psi_q + \dfrac{d\psi_d}{dt} \\ u_q = R_s i_q + \omega_e \psi_d + \dfrac{d\psi_q}{dt} \end{cases} \tag{2.12}$$

The flux equations in *d-q* coordinate are presented in (2.13). Since the phase *d* is assigned along the rotor. The total flux in phase *d* is the combination of stator flux and rotor flux. In (2.13), ψ_f represents the rotor flux.

$$\begin{cases} \psi_d = L_d i_d + \psi_f \\ \psi_q = L_q i_q \end{cases} \tag{2.13}$$

The electromagnetic torque equation in *d-q* coordinate is presented in (2.14). In (2.14), n_p is the number of pole pairs.

$$T_e = \frac{3}{2} n_p \left(\psi_d i_q - \psi_q i_d \right) \tag{2.14}$$

According to Newton's second law, the torsional mechanical equation is present in (2.15). In (2.15), ω_m represents rotor mechanical speed, *J* represents the moment of inertia, T_L represents the load torque (T_L is constant) and *B* represents friction.

$$\frac{d\omega_m}{dt} = \frac{1}{J} \left(T_e - T_L - B\omega_m \right) \tag{2.15}$$

The relationship between electrical speed and mechanical speed is shown in (2.16).

$$\omega_e = n_p \omega_m \tag{2.16}$$

2.5 Field Oriented Control (FOC)

FOC is the decoupling control strategy for PMSM and the control methods such as PI, FLC and SMC can be applied to PMSM based on the control frame of FOC.

The purpose of FOC on PMSM is to control the composite flux linkage and electromagnetic torque of PMSM separately, so that the control frame of PMSM can be simplified as the control frame of a separately excited DC motor [2].

The working principle of FOC is demonstrated in Figure 2.19. In Figure 2.19, ψ_S is the composite flux linkage, ψ_d and ψ_q are total flux linkage in phase *d* and phase *q*, L_d and L_q are self-induction in phase *d* and phase *q*, i_d and i_q are currents in phase *d* and phase *q*, ψ_f is the rotor flux, i_S represents the composite current vector, ω_e is the angular electrical speed and θ_e is the angular position.

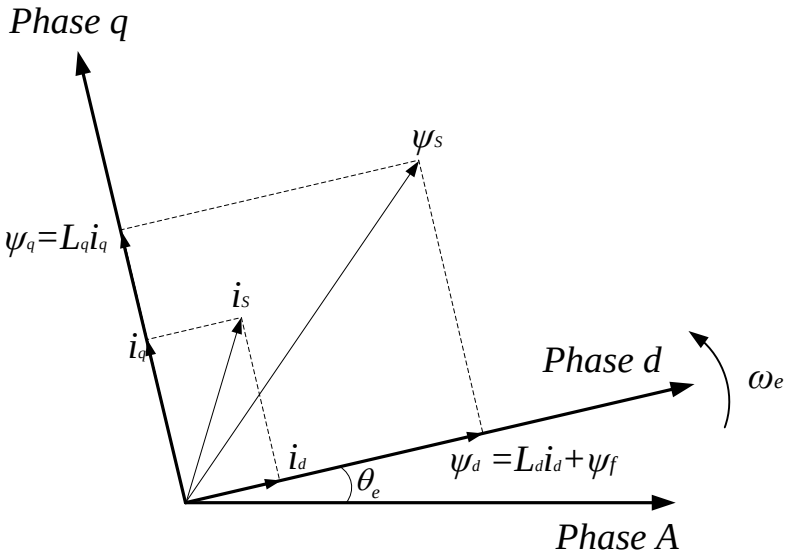

Figure 2.19: Demonstration of FOC

In the control frame of FOC the phase *d* current is controlled to be zero. When phase *d* current is zero, the total flux linkage in phase *d* is equal to the rotor flux linkage which is constant. Then the composite flux linkage ψ_S is only modified by the phase *q* flux linkage ψ_q and ψ_q is controlled by i_q.

The system can generate the maximum electromagnetic torque when the phase *d* current is zero. The (2.14) can be rewritten as (2.17). So the electromagnetic torque is controlled by phase *q* current i_q.

$$T_e = \frac{3}{2} n_p \psi_f i_q \tag{2.17}$$

For FOC realization, the phase *d* current and phase *q* current need to be controlled separately. So there are two current feedback control loops. And there is a speed feedback control loop in PMSM speed system.

The block diagram of PMSM speed system is shown in Figure 2.24. In Figure 2.24, ω_d is the speed reference signal, ω_m is the speed feedback signal, θ_m is the position feedback signal, *u* is speed control signal (*u* is also the reference signal for *q* current control loop), u_d is phase *d* current control signal, and u_q is phase *q* current control signal. Since the phase *d* current needs to be maintained at zero, the phase *d* reference is zero.

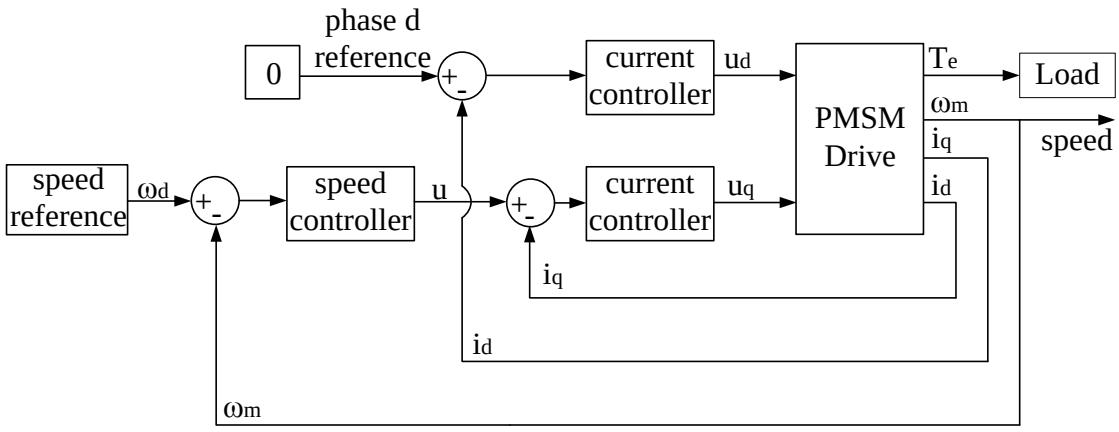

Figure 2.20: Block diagram of PMSM speed system

2.6 Summary

The mechanical structure of PMSM was introduced in this Chapter. The working principle of PMSM was discussed. The PMSM equivalent circuits and PMSM mathematical models were also presented, and the FOC working principle and control frame was introduced.

CHAPTER III

SLIDING MODE CONTROL

3.1 Concept of SMC

Sliding mode control (SMC) is a nonlinear control method which forces the states of a system to land and remain on the desired states trajectories with the control signal that switches in high frequency between positive and negative saturation.

SMC consists of three parts, which are sliding surface, switching control and equivalent control. Sliding surface is the desired states trajectories. Switching control is a discontinuous control law to force the states to land on the sliding surface from their initial conditions. Equivalent control is a continuous control law to remain the states on the sliding surface.

3.1.1 Sliding surface

Sliding surface is the essential part of SMC because it defines the desired states trajectories, which affects the stability and dynamic performance of the system.

For a n-th order single input single output system, the sliding surface is defined as (3.1) [58]. In (3.1), s represents the sliding surface, c is a positive scalar, which is the sliding surface coefficient, e is the tracking error, and n is the order of the system.

$$s = \left(\frac{d}{dt} + c \right)^{n-1} e \tag{3.1}$$

For a second order system, the sliding surface will be $s = \dot{e} + ce$ and its demonstration in phase plane is presented in Figure 3.1. In Figure 3.1, SMC should force any initial states to land on the sliding surface in a finite time. If both the tracking error and the derivative of the tracking error are zero, the system reaches the demanded states.

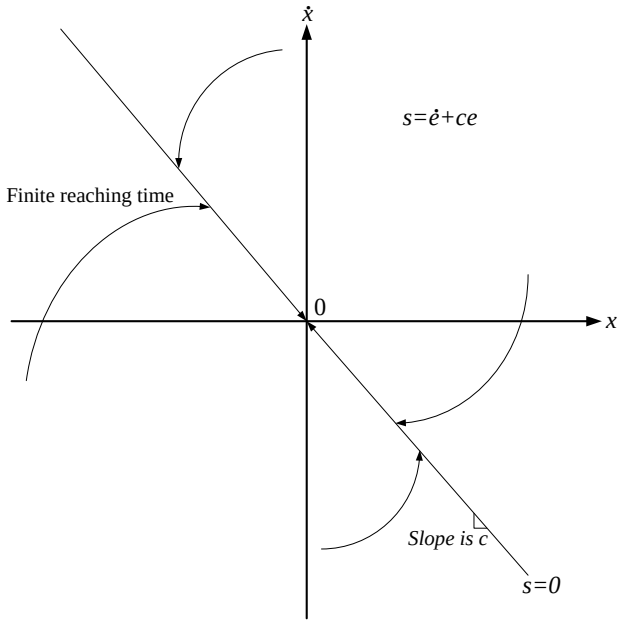

Figure 3.1: Example of sliding surface [45, 58]

Once the sliding surface is defined, the control problem concerning the system's dynamics is transferred to remaining the system's states on the sliding surface. The order of the sliding surface is less than the order of the system, so the sliding surface has the advantage of order reduction for control design.

The stability of SMC is testified using Lyapunov's second method for stability. Define a positive definite Lyapunov function as (3.2) [45]. In (3.2), V is a positive definite Lyapunov function and s is a sliding surface. If the derivative of (3.2) is a negative definite function as (3.3), the system is asymptotically stable in the sense of Lyapunov.

$$V(s) = \frac{1}{2}s^2 \geq 0, only V(0) = 0 \tag{3.2}$$

$$\dot{V}(s) = s\dot{s} < 0 \tag{3.3}$$

3.1.2 Switching control

Switching control is used to force the initial states of the system to land on the desired state trajectories in a finite time and also used to force the states back to the desired state trajectories when disturbances occur.

The switching control is defined as (3.4) [45]. In (3.4), u is the switching control law, u_o is the positive controller gain and s is the sliding surface. The switching control has only two output signals, and the sign of switching control is decided by the sign of the sliding surface. If the sliding surface is position, the switching control signal is positive. If the sliding surface is negative, the switching control signal is negative.

$$u = \begin{cases} +u_o \ if \ s > 0 \\ -u_o \ if \ s < 0 \end{cases} \tag{3.4}$$

The switching control can be written as (3.5) [45]. In (3.5), $\mathrm{sgn}(s)$ is a sign function that switches between 1 and -1 at high frequency.

$$u = u_o \,\mathrm{sgn}(s) \tag{3.5}$$

We take the first order relay system which is presented by (3.6) as an example to explain how switching control works [58]. In (3.6), *x* is the output signal, *u* is the control signal and $f(x)$ is an unknown but bounded function, and $|f(x)| < f_0$, where f_0 is constant.

$$\dot{x} = f(x) + u \tag{3.6}$$

The switching control effort u_{sw} for the system (3.6) is designed as (3.7). In (3.7), *e* is the tracking error and *r* is the reference signal.

$$u_{sw} = u_o \,\mathrm{sgn}(e) \tag{3.7}$$

$$e = r - x \tag{3.8}$$

The derivative of tracking error can be developed as (3.9). If the switching controller gain $u_o > (f_0 + |\dot{r}|)$, then $e\dot{e} < 0$. The error will decrease to zero at a finite time.

$$\dot{e} = \dot{r} - \dot{x} = \dot{r} - f(x) - u_o \,\mathrm{sgn}(e) \tag{3.9}$$

3.1.3 Equivalent control

Equivalent control is a continuous control used to keep the system states staying on the desired state trajectories.

Under the equivalent control, the system states would not drift out of the sliding surface unless there is unknown internal dynamics or external disturbance. Equivalent control is mainly designed to compensate the internal dynamics under the assumption that the major internal dynamics and system parameters are known.

We use the first order relay system in (3.6) as an example to explain equivalent control.

If the internal dynamic $f(x)$ can be estimated by a known function $\hat{f}(x)$, $f(x)$ can be cancelled by $\hat{f}(x)$ [58]. Inserting $\left(\hat{f}(x)-\dot{r}\right)$ into (3.9), yields (3.10).

$$\dot{e}=\dot{r}-\dot{x}=\dot{r}-f(x)+\left(\hat{f}(x)-\dot{r}\right)-u_o\,\mathrm{sgn}(e) \tag{3.10}$$

Define the difference between $f(x)$ and $\hat{f}(x)$ as $\Delta f=\left|\hat{f}(x)-f(x)\right|$. Then (3.10) can be rewritten as (3.11).

$$\dot{e}=\dot{r}-\dot{x}=\Delta f-u_o\,\mathrm{sgn}(e) \tag{3.11}$$

The error will decrease to zero if $u_o>\Delta f$ because $e\dot{e}<0$. Therefore the equivalent control can be designed as (3.12).

$$u_{eq}=-\hat{f}(x)+\dot{r} \tag{3.12}$$

The general equivalent control law can be calculated by letting the derivative of sliding surface $\dot{s}=0$.

3.2 SMC Design

We take a general second order system (3.13) as an example to explain SMC design. In (3.13), *y* is the system's output signal, *u* is the control signal, *b* is a scalar, and $f(\dot{y}, y, t)$ represents the system's dynamics, which is not exactly known but is bounded.

$$\ddot{y} = f(\dot{y}, y, t) + bu \tag{3.13}$$

The sliding surface is designed according to (3.1). Since it is a second order system, the sliding surface should be (3.14). In (3.14), *e* is the tracking error and defined by (3.15), and *r* is the reference signal.

$$s = \dot{e} + ce \tag{3.14}$$

$$e = r - y \tag{3.15}$$

Differentiating (3.14) and making the derivative of sliding surface equal to zero produces (3.16).

$$\dot{s} = \ddot{e} + c\dot{e} = 0 \tag{3.16}$$

Substituting (3.13) and (3.15) into (3.16), we will have (3.17). In (3.17), f represents $f(\dot{y}, y, t)$.

$$\dot{s} = (\ddot{r} - f - bu) + c\dot{e} = 0 \tag{3.17}$$

The equivalent control can be designed as (3.18). In (3.18), $\hat{f}$ is the estimation of $f(\dot{y}, y, t)$.

$$u_{eq} = \frac{1}{b}\left(\ddot{r} - \hat{f} + c\dot{e}\right) \tag{3.18}$$

The switching control is designed as (3.19). In (3.19), *k* is a positive controller gain.

$$u_{sw} = k\,\mathrm{sgn}\left(s\right) \tag{3.19}$$

The general SMC is the combination of equivalent control and switching control as (3.20).

$$u = u_{eq} + u_{sw} \tag{3.20}$$

Lyapunov's second method is used to testify the stability of SMC. Substituting (3.20) into (3.17), we can obtain (3.21).

$$\dot{s} = \left(\ddot{r} - f - b\left(u_{eq} + u_{sw}\right)\right) + c\dot{e} \tag{3.21}$$

Substituting (3.18) and (3.19) into (3.21), we have (3.22).

$$\dot{s} = \hat{f} - f - bk\,\mathrm{sgn}\left(s\right) \tag{3.22}$$

Define $\Delta f = \hat{f} - f$. Equation (3.22) can be rewritten as (3.23), where *bk* is defined as *K* in (3.24).

$$\dot{s} = \Delta f - K\,\mathrm{sgn}\left(s\right) \tag{3.23}$$

$$K = bk \tag{3.24}$$

The system will be stable in sense of Lyapunov if $K > \Delta f$ because $s\dot{s} < 0$.

3.3 Application of SMC to PMSM Speed System

The speed tracking error signal *e* is defined as the difference between reference speed ω_d and the speed feedback signal ω_m as (3.25).

$$e = \omega_d - \omega_m \tag{3.25}$$

Substituting (2.15) into the double derivative of the error signal *e*, we can obtain (3.26).

$$\ddot{e} = \ddot{\omega}_d - \ddot{\omega}_m = \ddot{\omega}_d - \left(\frac{3n_p\psi_f}{2J}\dot{i}_q - \frac{B}{J}\dot{\omega}_m \right) \tag{3.26}$$

We define the sliding surface as (3.27).

$$s = \dot{e} + ce \tag{3.27}$$

We calculate the equivalent controller for PMSM speed system by letting $\dot{s} = 0$ as represented by (3.28)

$$\dot{s} = \ddot{e} + c\dot{e} = \left(\ddot{\omega}_d - \frac{3n_p\psi_f}{2J}\dot{i}_q + \frac{B}{J}\ddot{\omega}_m \right) + c\dot{e} = 0 \tag{3.28}$$

The equivalent control is calculated as (3.29). In (3.29), i_q is the control signal for PMSM speed control loop. Parameter *b* is a scalar as (3.30).

$$u_{eq} = i_q = \frac{1}{b}\left(\dot{\omega}_d + \frac{B}{J}\dot{\omega}_m + ce \right) \tag{3.29}$$

$$b = \frac{3n_p\psi_f}{2J} \tag{3.30}$$

The switching control is designed as (3.31). In (3.31), K is the positive controller gain.

$$u_{sw} = K \operatorname{sgn}(s) \tag{3.31}$$

The SMC for PMSM speed control loop is the combination of equivalent control and switching control as in (3.28).

$$u = u_{eq} + u_{sw} = \frac{1}{b}\left(\dot{\omega}_d + \frac{B}{J}\dot{\omega}_m + ce \right) + K \operatorname{sgn}(s) \tag{3.32}$$

3.4 Summary

The basic concept of SMC has been introduced in this Chapter. Also the design procedure of SMC and its implementation on PMSM speed control were introduced.

CHAPTER IV

LINEAR ACTIVE DISTURBANCE REJECTION CONTROL

4.1 Concept of LADRC

ADRC is an advanced control technology, which is specialized on estimation and cancellation of system internal and external disturbances with the use of an extended state observer (ESO).

Linear ADRC or LADRC consists of the LESO and a general PD controller. As the major disturbance signals such as unknown internal dynamics and external load variation are cancelled, a complex system can be controlled by a general PD controller to achieve desired performances.

For LADRC design, only two factors need to be known. The first factor is the order of the system, which can be tested by time response or frequency response. The other factor is the basic parameters of the system, which can be acquired from manufacturer's data.

LESO offered the possibility of disturbance estimation for LADRC. The total internal unknown dynamics and external disturbance are considered as a generalized disturbance, which is estimated by an augment state [51] in LESO. Therefore, for a second-order system, we need a third-order LESO to estimate the system states.

The block diagram of LADRC with a third-order LESO is shown in Figure 4.1. In Figure 4.1, r is the reference signal and $\dot{r}$ is the derivative of r. Parameter e is the tracking error signal and $\dot{e}$ is the derivative of e. PD represents a general proportional-derivate controller. Parameter u_0 is the control signal for the ideal system dynamic after disturbance cancellation. Parameter b is a scalar for control input. Parameter u is the control signal. Parameter w represents the external disturbance. Paremeter y is the system's output signal. Patermeter z_1 is the estimation of y. Paremeter z_2 is the derivative of z_1. Parameter z_3 is the estimated generalized disturbance signal.

In Figure 4.1, the LESO takes the control signal u and feedback signal y as inputs, and it estimates y and the generalized disturbance signal with z_1 and z_3 respectively. The estimated total disturbance signal is used to cancel the real disturbance in the plant. After the disturbance cancellation, the plant can be controlled by a general PD controller.

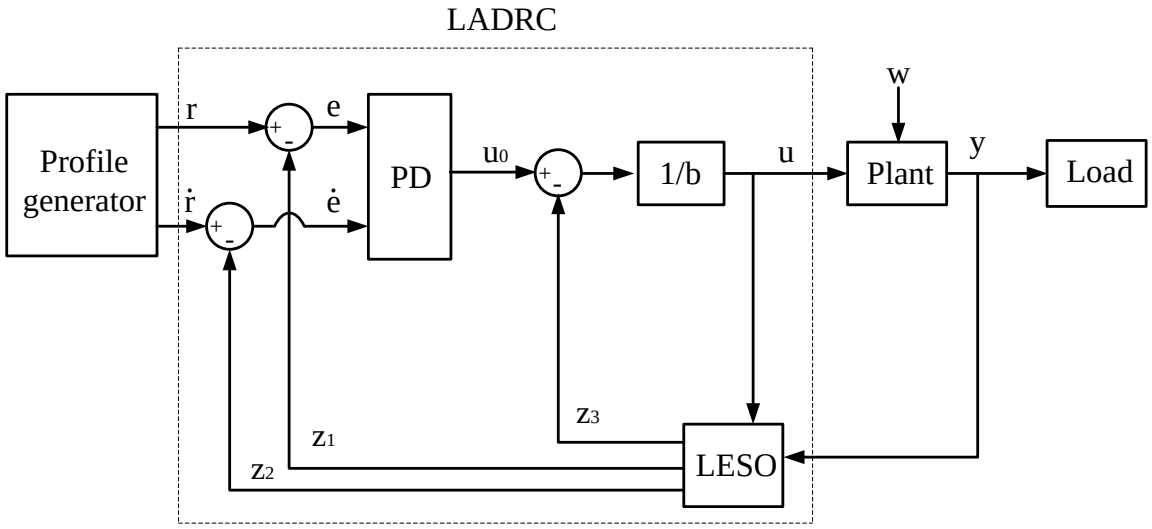

Figure 4.1: Block diagram of LADRC with a third-order LESO

4.2 LADRC Design

A generalized second order system (4.1) is taken as an example to explain the LADRC design [51]. In (4.1), y is the output signal, u is the control signal. $f\left(\dot{y}, y, w, t\right)$ represents the system dynamics that contain the internal and external disturbances, w is external disturbances, t is time and b is constant.

$$\ddot{y} = f\left(\dot{y}, y, w, t\right) + bu \tag{4.1}$$

For motion control systems, b is the torque constant that is related to moment of inertia, which can be calculated by designer [59].

In order to design LESO, (4.1) has to be written in state space form. Let $x_1 = y$, $x_2 = \dot{y}$ and $x_3 = f$ where f is an augmented state that is assumed to be differentiable. And let $h = \dot{f}$ and assume h is bounded.

Then the system (4.1) can be represented by state equations (4.2).

$$\begin{cases} \dot{x} = Ax + Bu + Eh \\ y = Cx \end{cases} \tag{4.2}$$

where $A = \begin{bmatrix} 0 & 1 & 0 \\ 0 & 0 & 1 \\ 0 & 0 & 0 \end{bmatrix}$, $B = \begin{bmatrix} 0 \\ b \\ 0 \end{bmatrix}$, $C = \begin{bmatrix} 1 & 0 & 0 \end{bmatrix}$ and $E = \begin{bmatrix} 0 \\ 0 \\ 1 \end{bmatrix}$.

For a second-order system, a third-order LESO is constructed as (4.3). In (4.3), z is the estimation of x, z_1 is the estimated feedback signal, z_2 is the derivative of z_1 and z_3 is the estimated total disturbance signal, L is the observer gain vector, and β_1, β_2 and β_3 are observer gains. The observer gain vector needs to be determined to make sure the observer poles are placed properly.

$$\begin{cases} \dot{z} = Az + Bu + L\left(x_1 - z_1\right) \\ \hat{y} = Cz \end{cases} \tag{4.3}$$

$$L = \begin{bmatrix} \beta_1 \\ \beta_2 \\ \beta_3 \end{bmatrix} \tag{4.4}$$

If all the poles of LESO are placed at $-\omega_o$ the tuning of LESO is simplified [51]. So the observer gain vector can be designed as (4.5). In (4.5), ω_o is the bandwidth of LESO [51].

$$L = \begin{bmatrix} \beta_1 \\ \beta_2 \\ \beta_3 \end{bmatrix} = \begin{bmatrix} 3\omega_o \\ 3\omega_o^2 \\ \omega_o^3 \end{bmatrix} \tag{4.5}$$

The LADRC control law is designed as (4.6). In (4.6), u is LADRC control law, u_o is the control signal for the ideal system dynamic after disturbance cancellation, z_3 is the estimated total disturbance signal and b is a scalar.

$$u = \frac{u_o - z_3}{b} \tag{4.6}$$

Substituting (4.6) into (4.1), we have (4.7).

$$\ddot{y} = f - z_3 + u_o \tag{4.7}$$

If the total disturbance f is estimated by z_3 accurately, it can be cancelled. Then the system (4.1) becomes a pure double integrator as (4.8) which is the ideal dynamic after disturbance cancellation.

$$\ddot{y} = u_o \tag{4.8}$$

For (4.8), u_o can be designed as a general PD controller given by (4.9). In (4.9), k_p and k_d are proportional and derivative controller gains respectively, r is the reference signal. z_1 is the estimated feedback signal and z_2 is the derivative of z_1.

$$u_o = k_p\left(r - z_1\right) + k_d\left(\dot{r} - z_2\right) \tag{4.9}$$

The tuning of u_o will be simplified by placing both the close-loop system poles at $-\omega_c$ [51]. So the controller gains in (4.9) can be designed as (4.10) and (4.11) [51].

$$k_p = \omega_c^2 \tag{4.10}$$

$$k_d = 2\omega_c \tag{4.11}$$

4.3 Application of LADRC to PMSM Speed System

The speed loop of PMSM is an approximate first-order system, so the first-order LADRC with a second-order LESO is applied to the loop.

Substituting (2.17) into (2.15), the differential equation of PMSM speed control loop is presented in (4.12). In (4.12), ω_m is the mechanical speed output, J is the moment of inertia, n_p is the number of pole pairs, ψ_f is the rotor flux linkage, i_q is phase q current, T_L is load torque, and B is friction factor.

$$\frac{d\omega_m}{dt} = \frac{1}{J}\left(\frac{3}{2}n_p\psi_f i_q - T_L - B\omega_m\right) \tag{4.12}$$

In (4.12), the generalized disturbance f is represented by (4.13).

$$f = -\frac{B}{J}\omega_m - \frac{T_L}{J} \tag{4.13}$$

Substituting (4.13) into (4.12), we have (4.14). In (4.14), b is defined by (3.30).

$$\frac{d\omega_m}{dt} = f + bi_q \tag{4.14}$$

Write (4.14) in state space form and we have (4.15). Let $x_1 = \omega_m$, $x_2 = f$ and $\dot{f} = h$. In (4.15), x is the state vector, u is the control vector and h is an augment vector.

$$\begin{cases} \dot{x} = Ax + Bu + Eh \\ y = Cx \end{cases} \tag{4.15}$$

where $A = \begin{bmatrix} 0 & 1 \\ 0 & 0 \end{bmatrix}$, $B = \begin{bmatrix} b \\ 0 \end{bmatrix}$, $C = \begin{bmatrix} 1 & 0 \end{bmatrix}$ and $E = \begin{bmatrix} 0 \\ 1 \end{bmatrix}$.

The LESO for (4.15) is designed as (4.16). In (4.16), z is the estimation of x, z_1 is the estimated feedback signal and z_2 is the estimated generalized disturbance. The observer gain vector L is designed as (4.17).

$$\begin{cases} \dot{z} = Ax + Bu + L\left(x_1 - z_1\right) \\ \hat{y} = Cz \end{cases} \tag{4.16}$$

$$L = \begin{bmatrix} 2\omega_o \\ \omega_o^2 \end{bmatrix} \tag{4.17}$$

The control law is designed as (4.18). In (4.18), i_q is the phase q current control signal.

$$u = i_q = \frac{u_o - z_2}{b} \tag{4.18}$$

The ideal dynamic of (4.14) after the disturbance cancellation is presented in (4.19).

$$\frac{d\omega_m}{dt} = u_o \tag{4.19}$$

The controller for (4.19) is designed as (4.20). In (4.20), ω_d is the speed reference signal and $\hat{\omega}_m$ is the estimated speed feedback signal.

$$u_o = k_p\left(\omega_d - \hat{\omega}_m\right) \tag{4.20}$$

4.4 Summary

The design process of LADRC is introduced in this chapter. The tuning of LADRC and LESO are explained. The application of LADRC to a first-order PMSM speed loop is discussed.

CHAPTER V

SIMULATION AND COMPARISON

5.1 Introduction

Matlab is powerful software that can solve complex mathematical problems. Simulink is an important toolbox of Matlab, which shares the calculation ability of Matlab and provides the possibility of graphic modeling. Graphic modeling helps the designers build models that represent the real world systems in structure and function. The design in Matlab/Simulink does not have to run the real-world systems but with the major problems being solved, which lowers the research cost. So it is broadly used in science and engineering research.

In this Chapter, the simulation results of PI controller, SMC and LADRC are presented in Section 5.2. The comparisons of PI controller, LADRC and SMC are presented in Section 5.3. The effectiveness of SMC and LADRC on a PMSM system is verified by simulation results.

5.2 Simulation Results

The PMSM parameters are presented in Table I.

TABLE I: PMSM PARAMETERS VALUES [60]

Name	Symbol	Value
Stator resistance	R_S	$2.875\,Ohm$
Rotor flux linkage	ψ_f	$0.175\,Wb$
Phase *d* inductance	L_d	$0.0085H$
Phase *q* inductance	L_q	$0.0085H$
Moment of inertia	J	$0.0008\,kgm^2$
Number of pole pairs	n_p	4
Rated speed	n	$3000\,rpm$

PI controller is a simple control method for PMSM speed system and it is broadly used in industry. So we consider the performance of PMSM speed system with PI speed controller as a reference performance for the performance of PMSM speed systems with SMC and LADRC.

The block diagram of PMSM speed system with PI controller is presented in Figure 5.1. In Figure 5.1, ω_d is the speed reference signal, ω_m is the speed feedback signal, *e* is the speed tracking error, *u* is the output of speed controller, u_d is the output of phase *d* current controller, u_q is the output of phase *q* current controller, T_e is electromagnetic torque, i_d is the current in phase *d* and i_q is the current in phase *q*. There

are speed feedback control loop and the current feedback control loop in Figure 5.1. The current feedback control loop is used to remain the PMSM currents and the speed controller is used to regulate the speed.

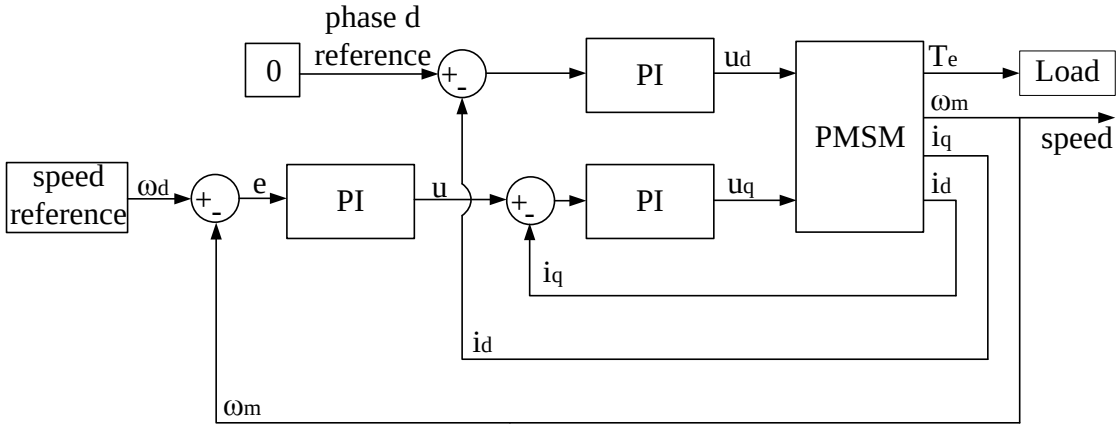

Figure 5.1: Block diagram of PMSM speed system with PI controllers

To decide the controller gains for current control loops, a small step input with a magnitude of $0.1\,A$ is used as reference signal for the current control loop. The current controller gains are decided as $k_p = 20$ and $k_i = 10$. The step responses for currents i_d and i_q with PI controllers are presented in Figure 5.2.

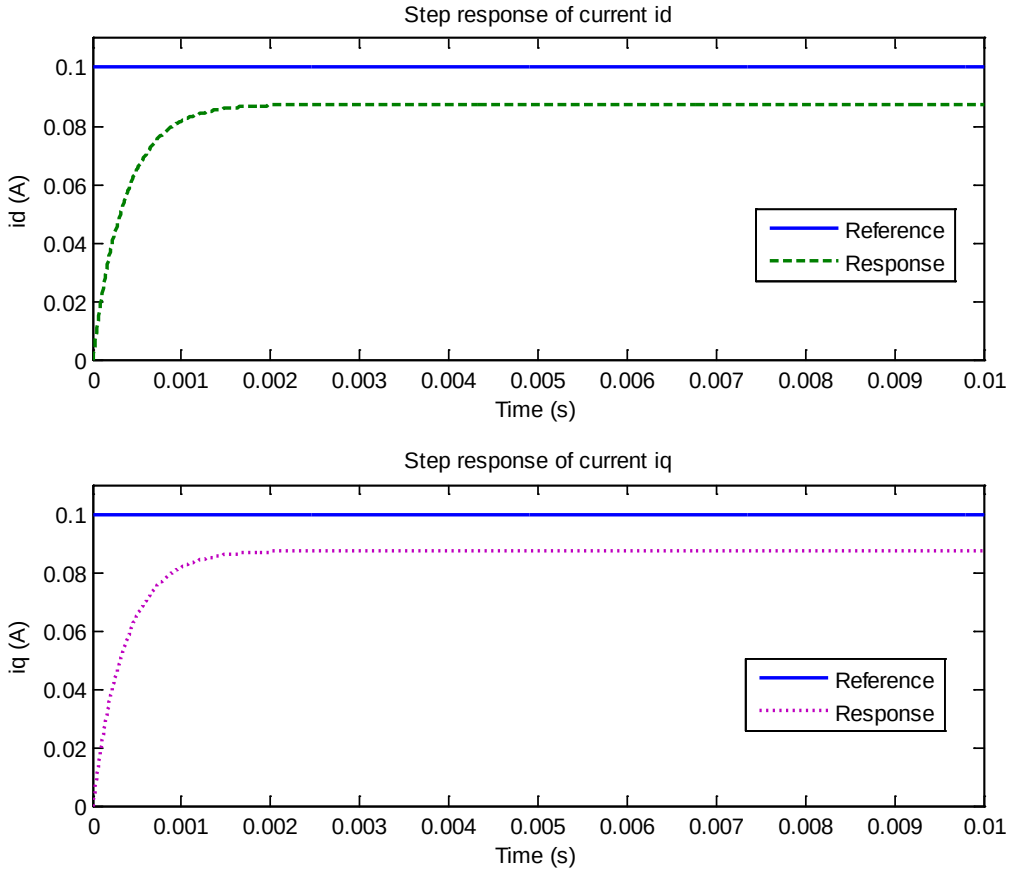

Figure 5.2: Step responses for current i_d and i_q with PI controllers

From Figure 5.2, we can see that the responses of current control loops are very fast. It takes approximately 0.002 seconds for the currents i_d and i_q to reach steady states. Advanced controllers are not usually applied to the current control loop because of the complex algorithms which could lengthen the responding time of the system. From the figure, we can also see that there are steady state errors in the step responses of the currents. However, the steady state error in current control loop will not affect the overall performance of PMSM speed system because this small error can be compensated by the speed controller.

We apply the PI controller to the speed control loop. The speed reference is a step input with magnitude of 200 *rad/s*. The controller gains $k_p = 0.5$ and $k_i = 11$ are decided by trial-and-error tuning in order to eliminate overshoot or steady state error in the step responses for speed feedback control loop.

The speed response of PMSM speed system with PI speed controller and PI control signal in the absence of load are presented in Figure 5.3.

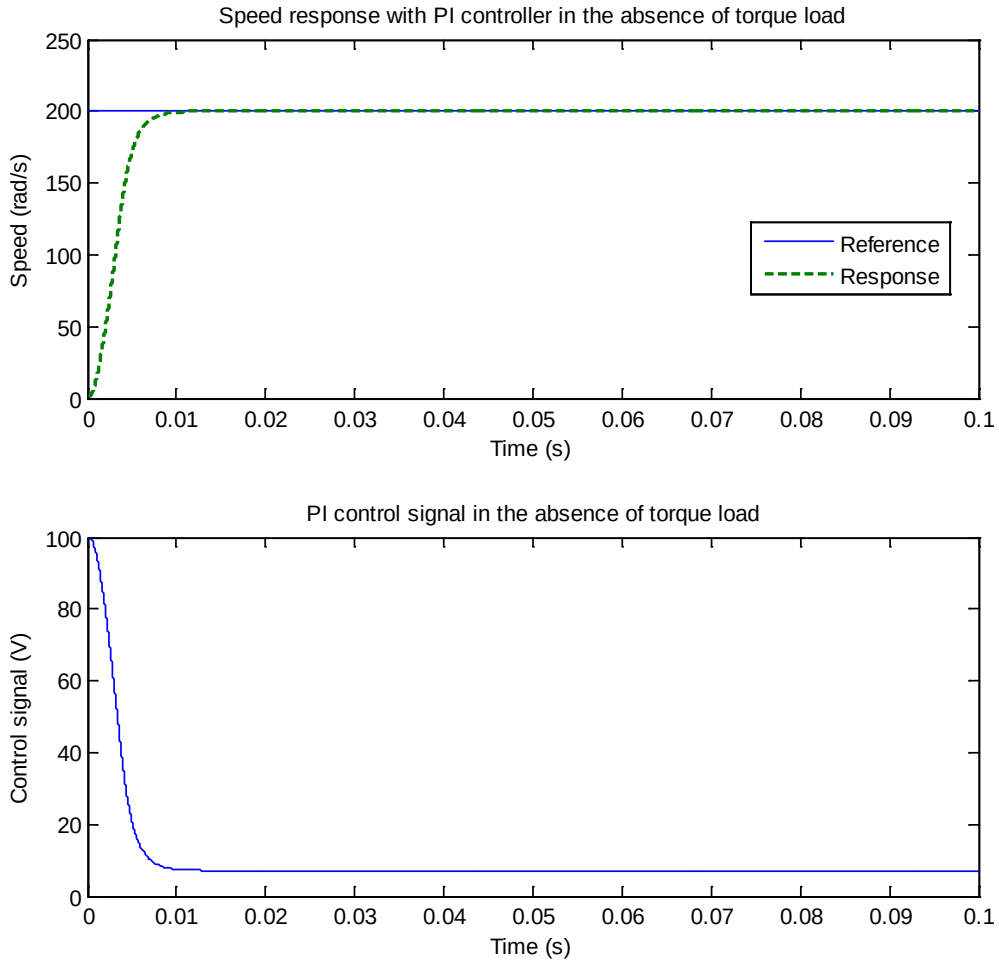

Figure 5.3: Speed response and PI control signal in the absence of torque load

From Figure 5.3, we can see that it takes 0.01 seconds for the speed to reach the set-point. The control signal remains at 7 *V* at steady state.

A step torque load with magnitude of 10 *Nm* is applied to the system at 0.1 second to test the PI controller's disturbance rejection capacity. The speed response and PI control signal in the presence of step torque load is presented in Figure 5.4.

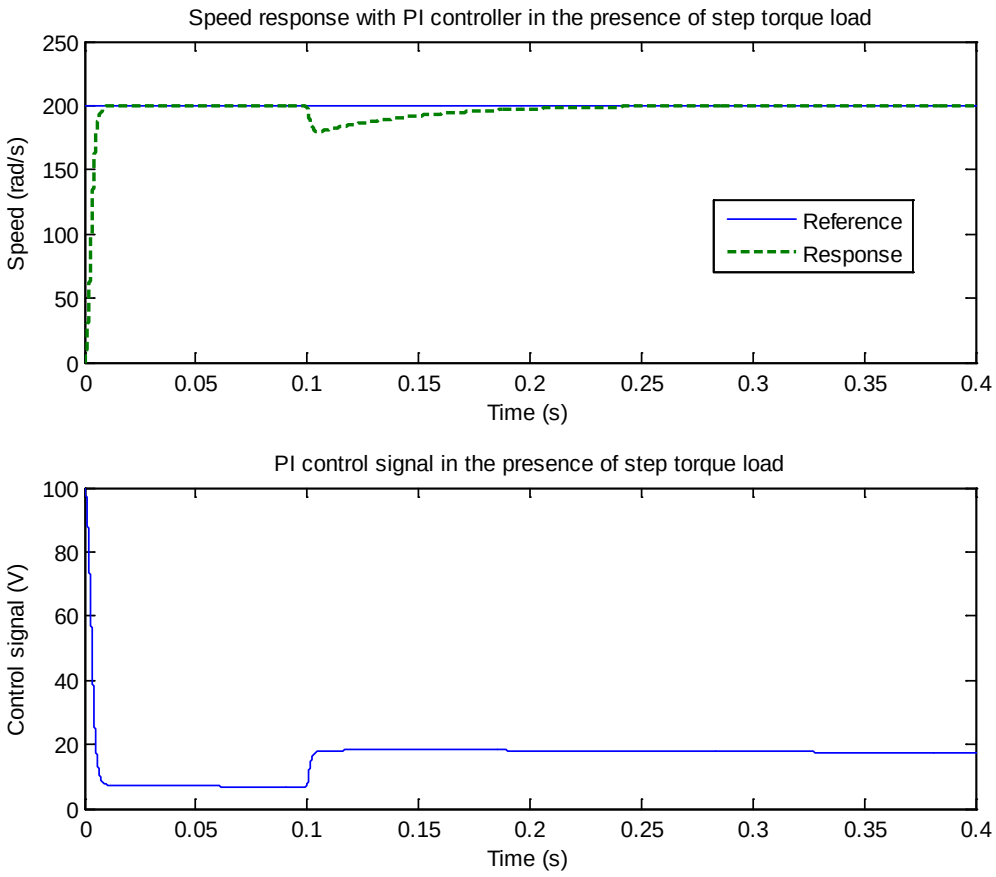

Figure 5.4: Speed response and PI control signal in the presence of torque load

From Figure 5.4, we can see that the speed drops 10 percent after the step load is applied. It takes 0.15 second for PI speed controller to drive the speed back to the set-point. The control signal increases to 18 *V* at steady state after the step load is applied.

Next we increase the moment of inertia five times to test the PI speed controller's robustness against parameter variations. The speed response and PI control signal with increased inertia are presented in Figure 5.5.

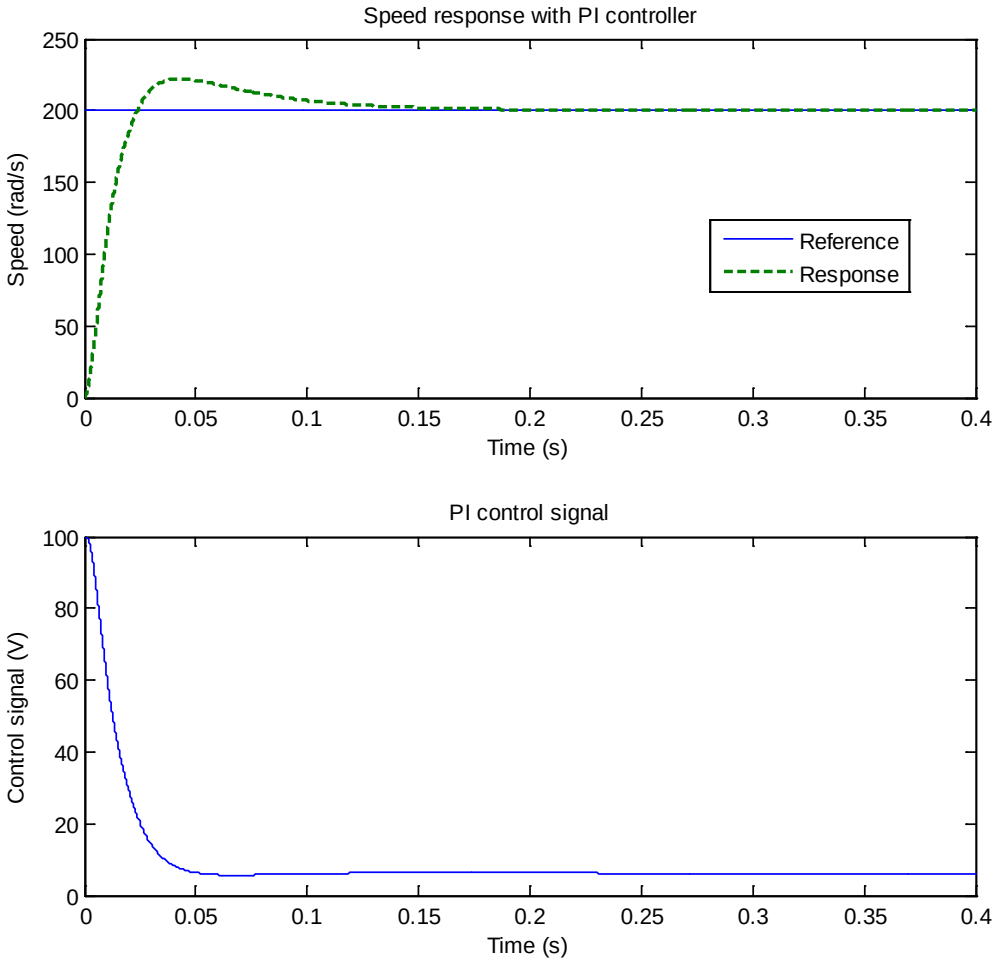

Figure 5.5: Speed response and PI control signal with increased moment of inertia

From Figure 5.5, we can see that the speed response has 11 percent overshoot after the moment of inertia is increased five times. And it takes 0.15 second for the PI speed control to drive the speed output to its steady state. The moment of inertia has the tendency to resist the change in motion. As the moment of inertia is increased, the

controller makes more effort to drive the speed to its set-point, resulting in over compensation.

The block diagram of PMSM speed system with SMC is presented in Figure 5.6. In Figure 5.6, PI controllers are applied to the currents control loops and the PI controller gains remain the same ($k_p = 20$ and $k_i = 10$). The SMC is applied to the speed control loop.

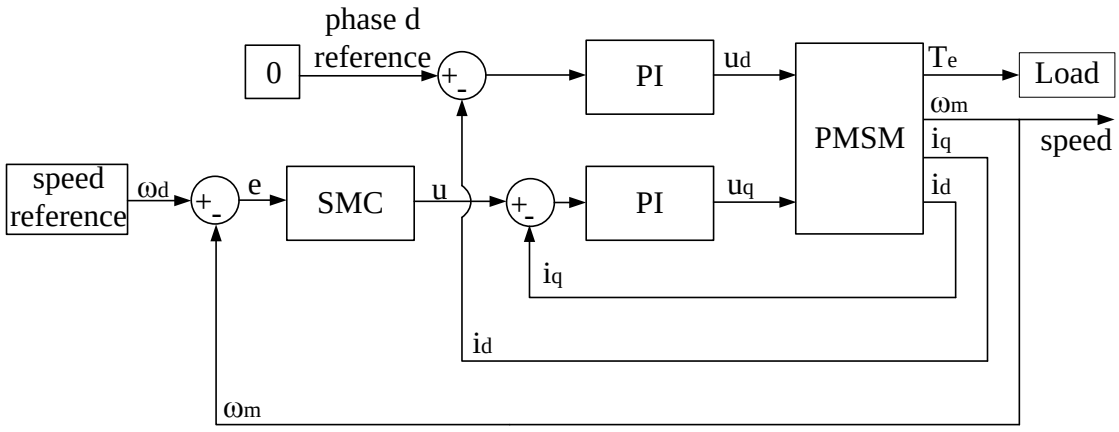

Figure 5.6: Block diagram of PMSM speed system with SMC

The SMC parameters are decided by trial-and-error tuning. The sliding surface coefficient is chosen as *c*=500 and the SMC controller gain is selected as *K*=20.

The speed response and SMC control signal without load are presented in Figure 5.7. The close view of the control signal of SMC in the absence of load is presented in Figure 5.8.

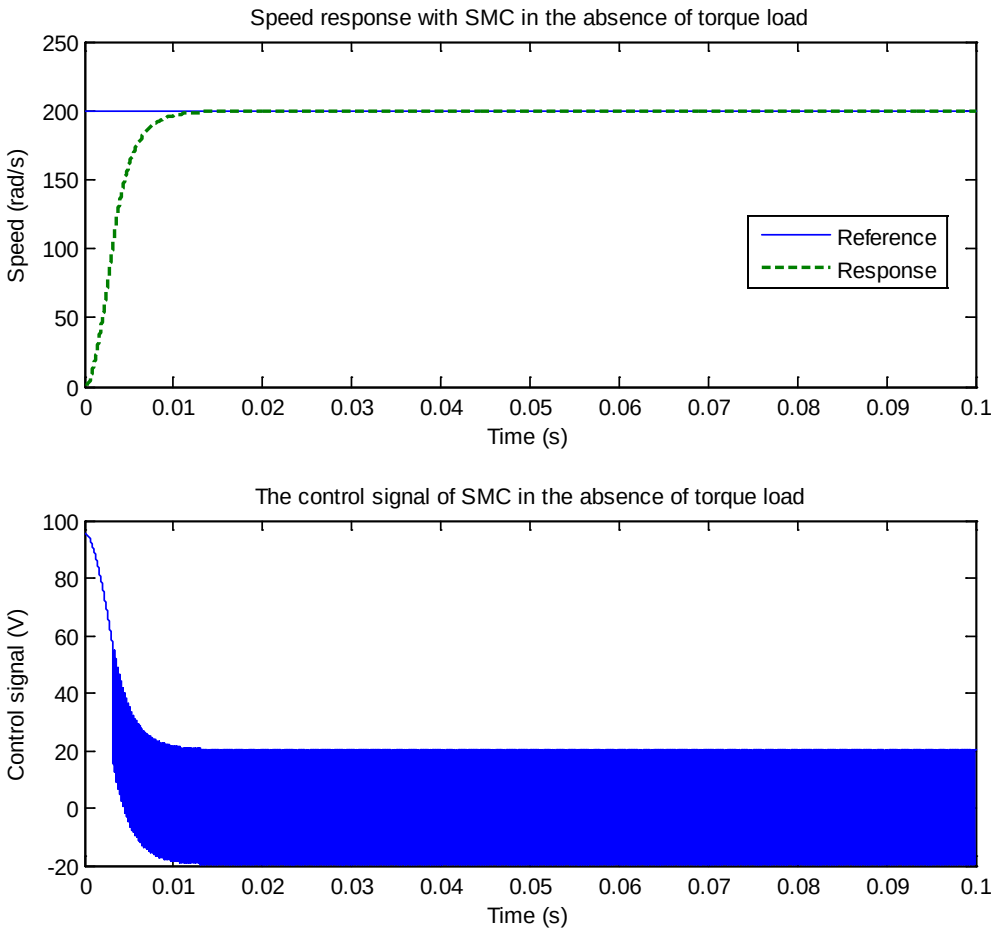

Figure 5.7: Speed response and the control signal of SMC in the absence of torque load

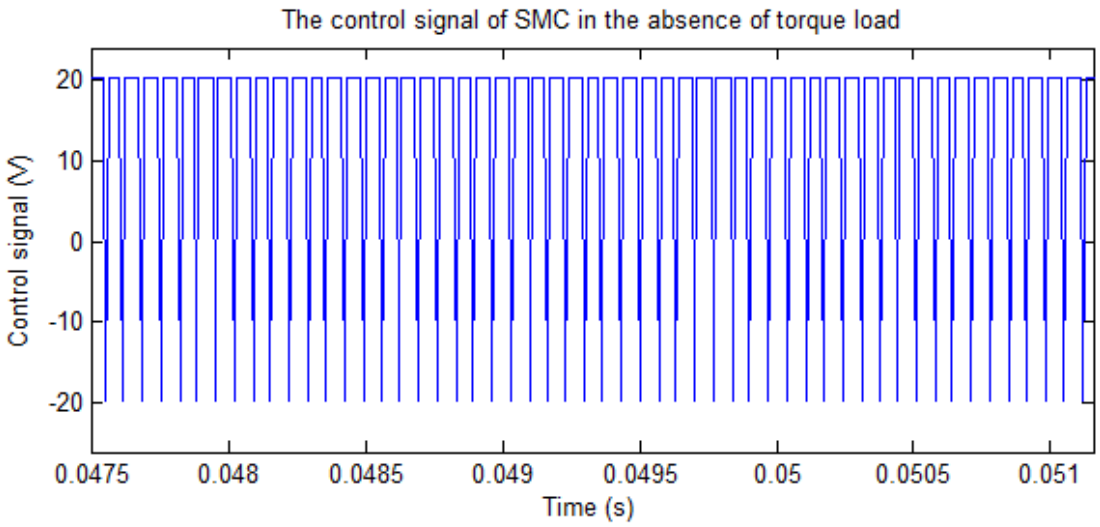

Figure 5.8: Close view of the control signal of SMC in the absence of torque load

From Figure 5.7, we can see that it takes 0.015 seconds for the speed output to reach the set-point. From Figure 5.8, we can see that control signal switches between 20 *V* and -20 *V* at steady state.

The same step torque load with magnitude of 10 *Nm* is applied to the system at 0.1 second to test the SMC's robustness against external disturbance. The speed response and SMC control signal in the presence of step torque load are presented in Figure 5.9.

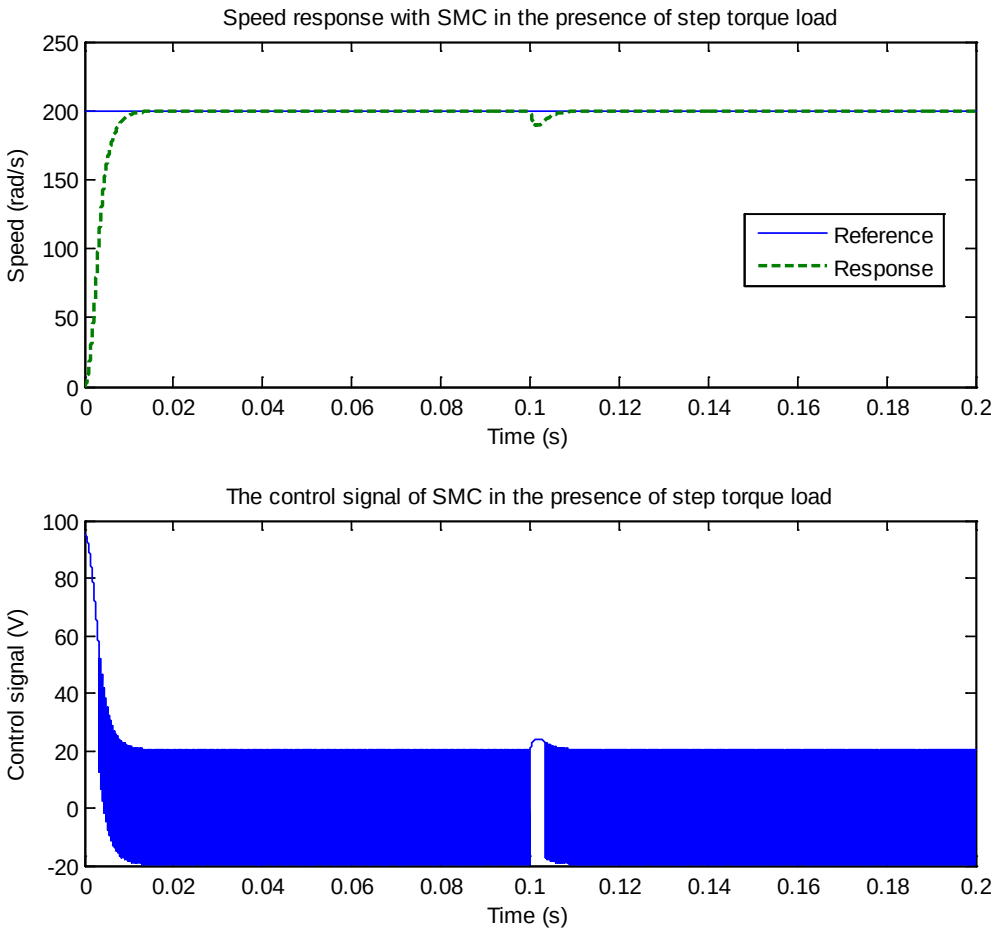

Figure 5.9: Speed response and the control signal of SMC in the presence of step torque load

The close view of the control signal of SMC in the presence of step torque load is presented in Figure 5.10.

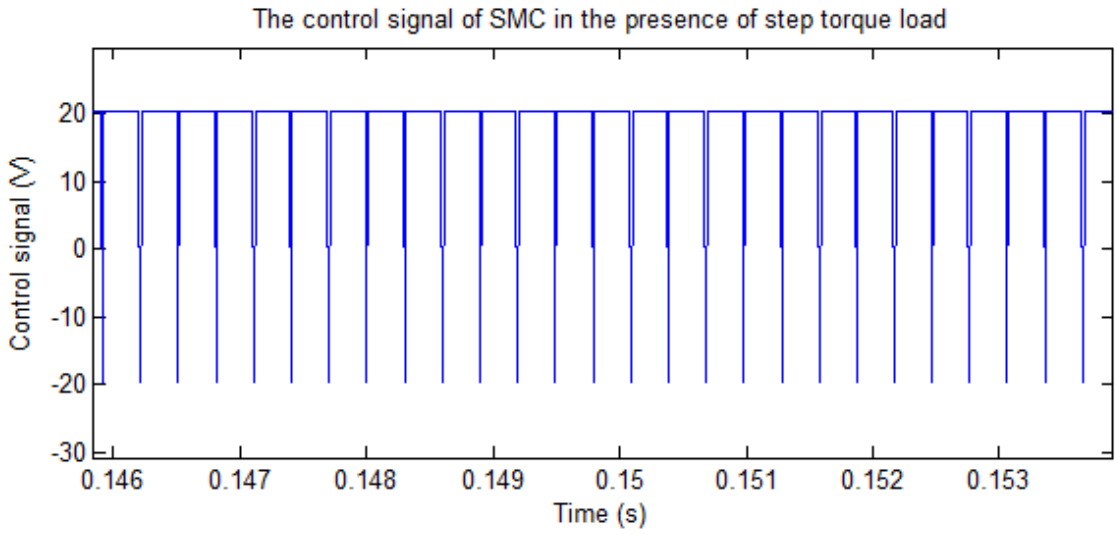

Figure 5.10 Close view of the control signal of SMC in the presence of step torque load

From Figure 5.9, we can see that the speed drops 5 percent after the step load is applied. It takes 0.01 seconds for SMC to drive the speed back to the set-point. The control signal still switches between 20 *V* and -20 *V* at steady state after the step load is applied.

Then we increase the moment of inertia five times to test the robustness of SMC against parameter variations. The speed response and SMC control signal with increased inertia are presented in Figure 5.11.

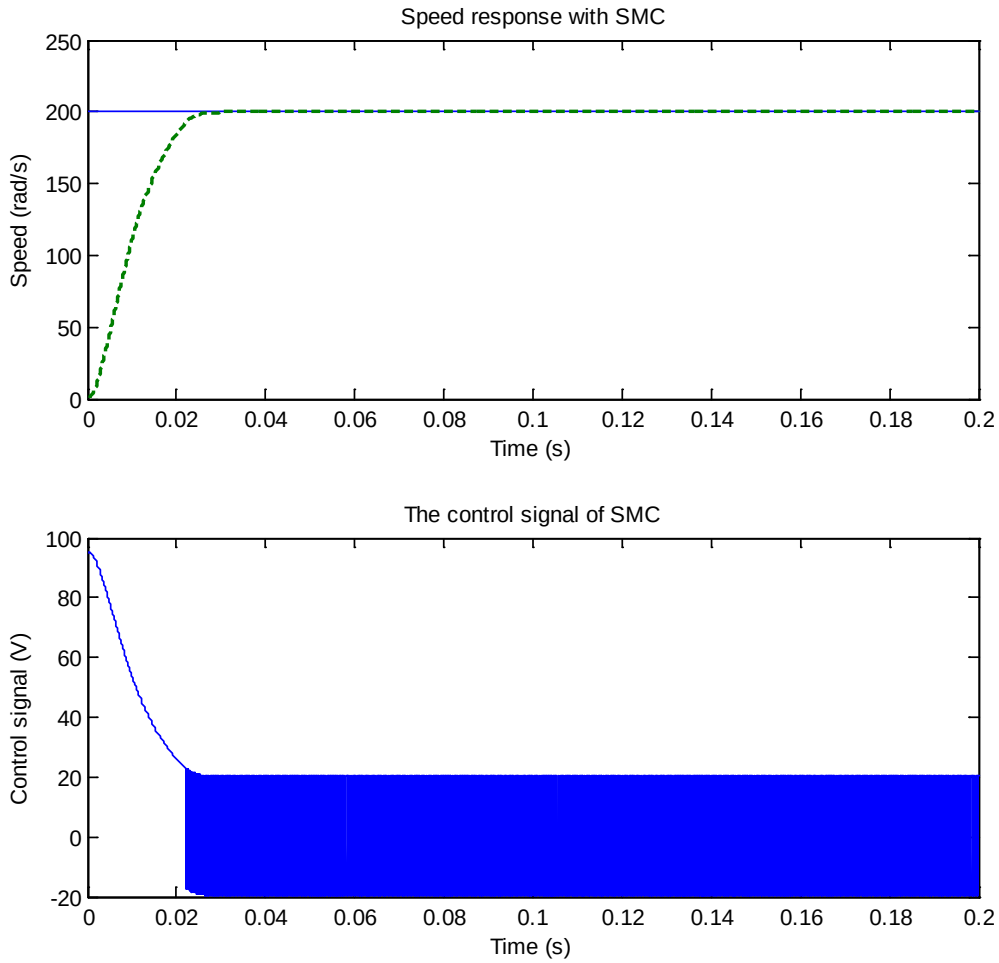

Figure 5.11: Speed response and the control signal of SMC with increased moment of inertia

The close view of the control signal of SMC with increased moment of inertia is presented in Figure 5.12.

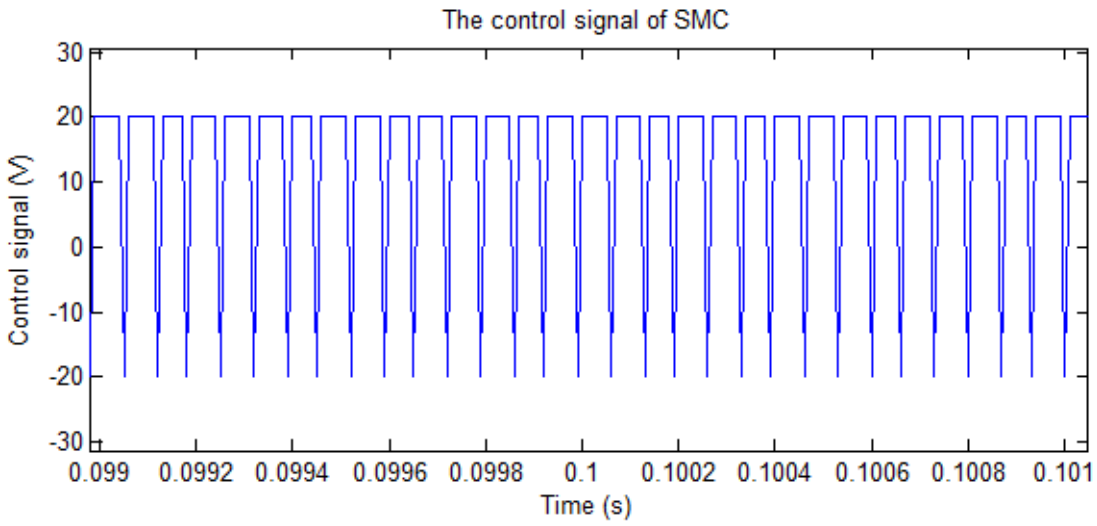

Figure 5.12 Close view of the control signal of SMC with increased moment of inertia

From Figure 5.11, we can see that there is no overshoot in the speed response. But it takes longer time (0.03 second) for the SMC to drive the speed to set-point. The SMC control signal still switches between 20 *V* and -20 *V* at steady state.

The block diagram of PMSM speed system with LADRC is presented in Figure 5.13. In Figure 5.13, PI controllers are applied to the currents control loops and the PI controller gains remain the same ($k_p = 20$ and $k_i = 10$). The LADRC is applied to the speed control loop.

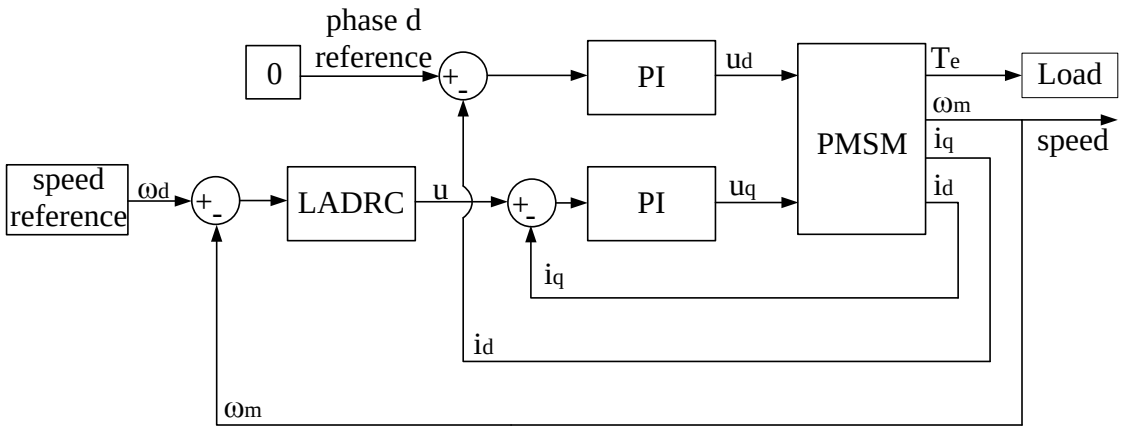

Figure 5.13: Block diagram of PMSM speed system with LADRC

The LADRC parameters are decided by trial-and-error tuning. The observer bandwidth is selected as $\omega_o = 900$ and the controller bandwidth is chosen as $\omega_c = 350$. The torque constant is *b*=1325.

The speed response and the control signal of LADRC in the absence of torque load are presented in Figure 5.14.

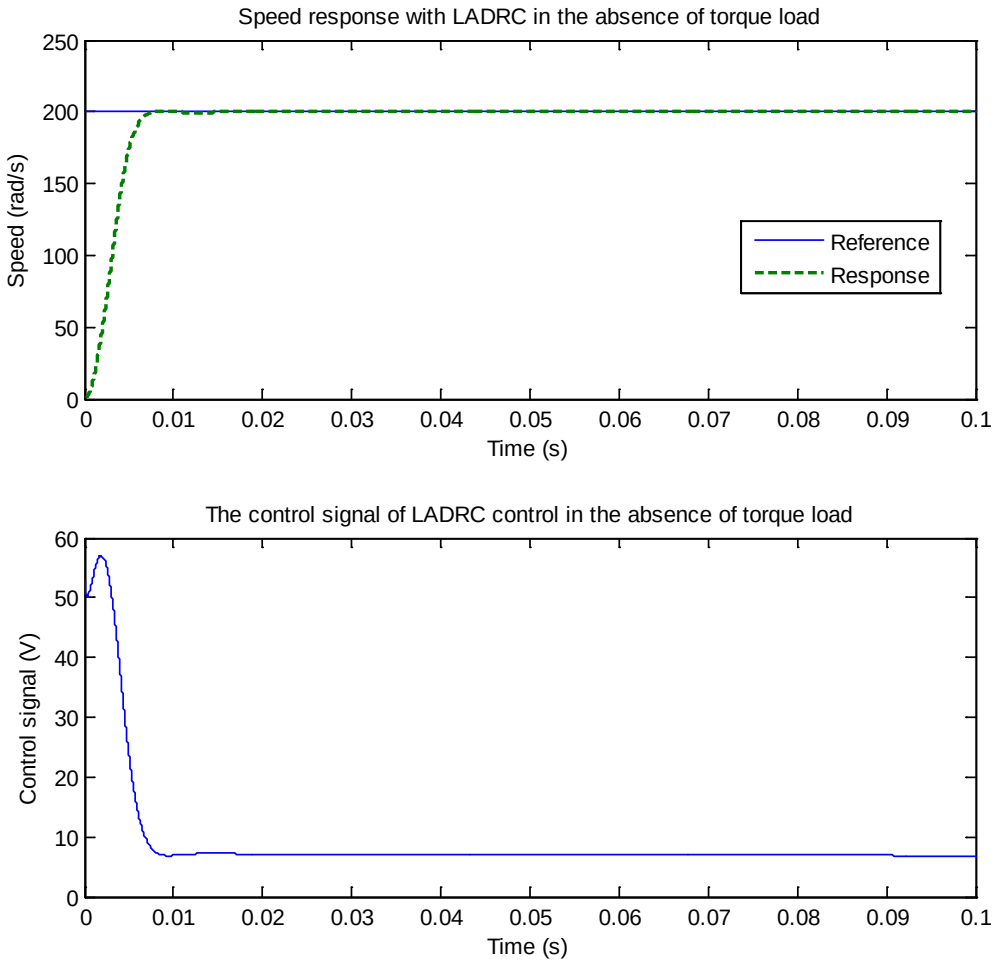

Figure 5.14: Speed response and the control signal of LADRC in the absence of torque load

From Figure 5.14, we can see that it only takes 0.007 seconds for the speed output to reach the set-point at. The control signal remains 7 *V* at the steady state.

The same step torque load with magnitude of 10 *Nm* is applied to the system at 0.1 second to test the robustness of LADRC against disturbance. The speed response and LADRC control signal with torque load are presented in Figure 5.15.

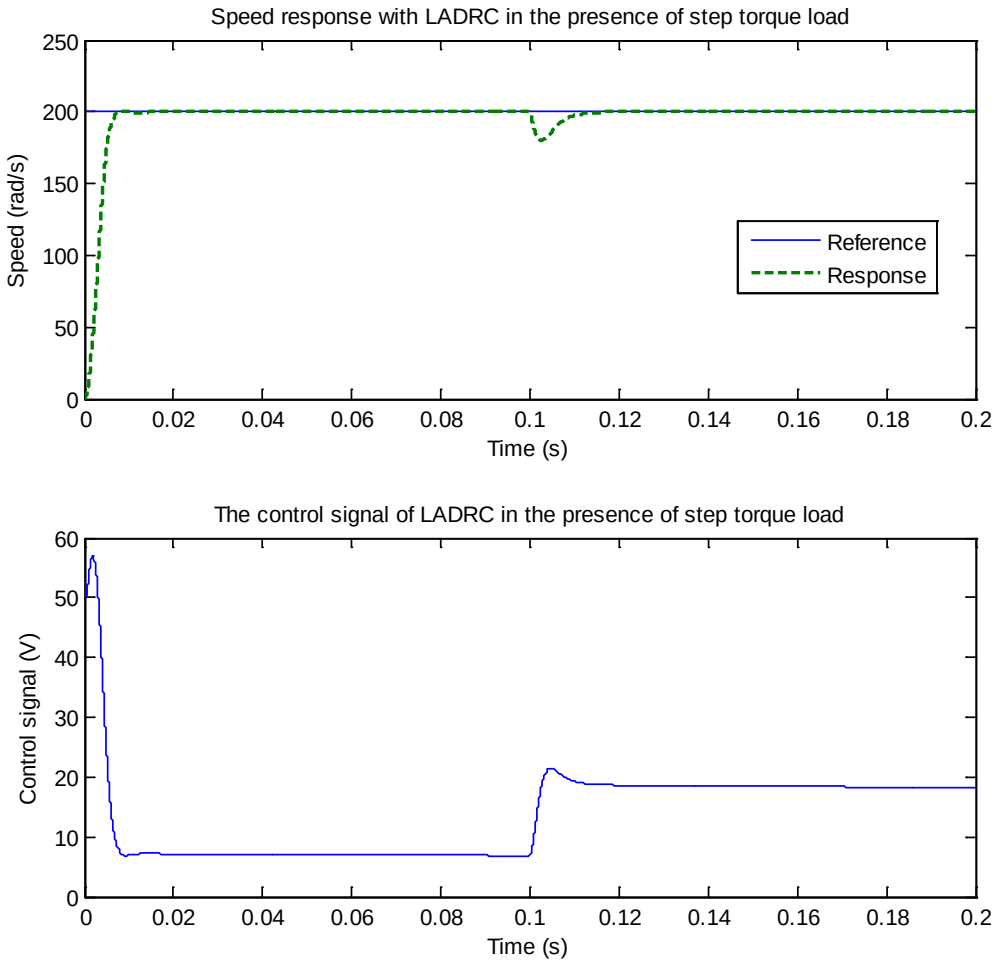

Figure 5.15: The speed response and the control signal of LADRC in the presence of step torque load

From Figure 5.15, we can see that the speed drops 10 percent after the step load is applied. It takes 0.01 second for LADRC to drive the speed back to the set-point. The control signal increases to 18 *V* at steady state after the step load is applied.

Next we increase the moment of inertia five times to test the robustness of LADRC against parameter variations. The speed response and the control signal of LADRC with increased inertia are presented in Figure 5.16.

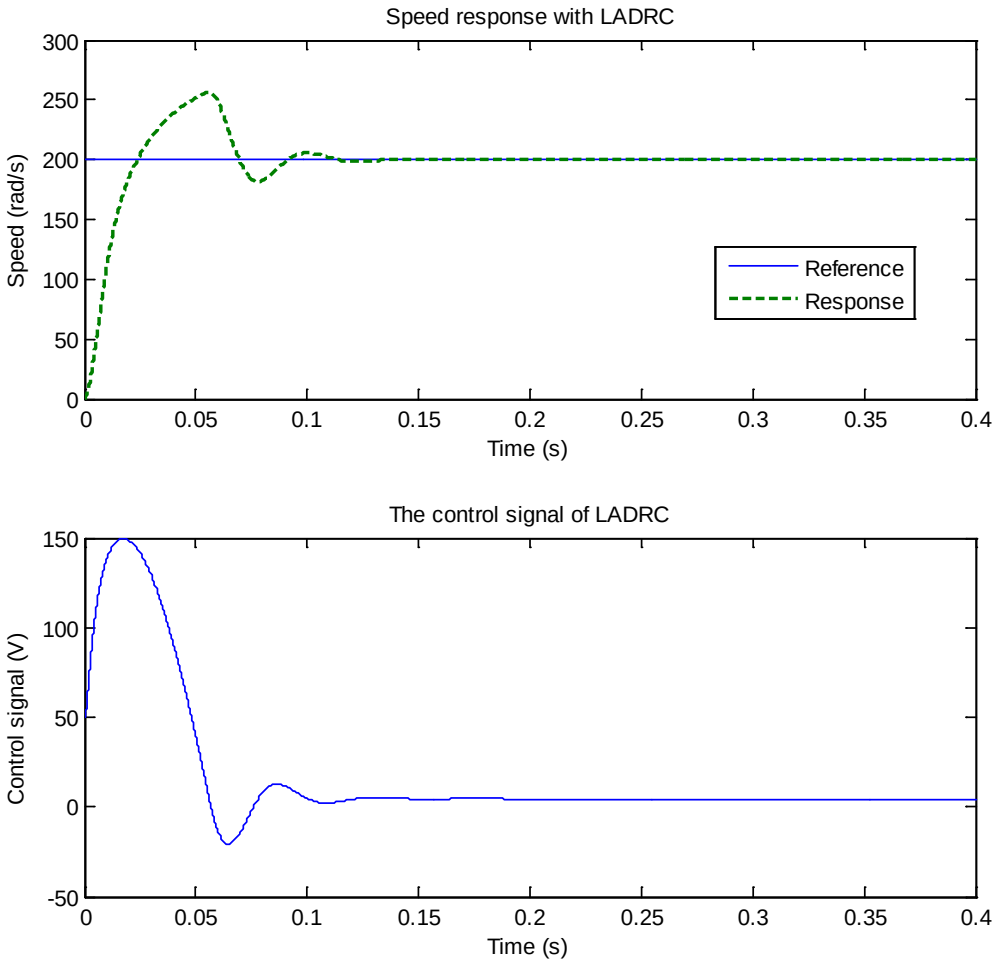

Figure 5.16: Speed response and the control signal of LADRC with increased moment of inertia

From Figure 5.16, we can see that there is 28 percent overshoot in the speed response. And it takes 0.15 second for the LADRC to drive the speed to steady state in the presence of increased moment of inertia.

Now we compare the speed responses of the PMSM speed system with PI controller, LADRC and SMC in the absence of torque load in one figure, which is presented in Figure 6.17.

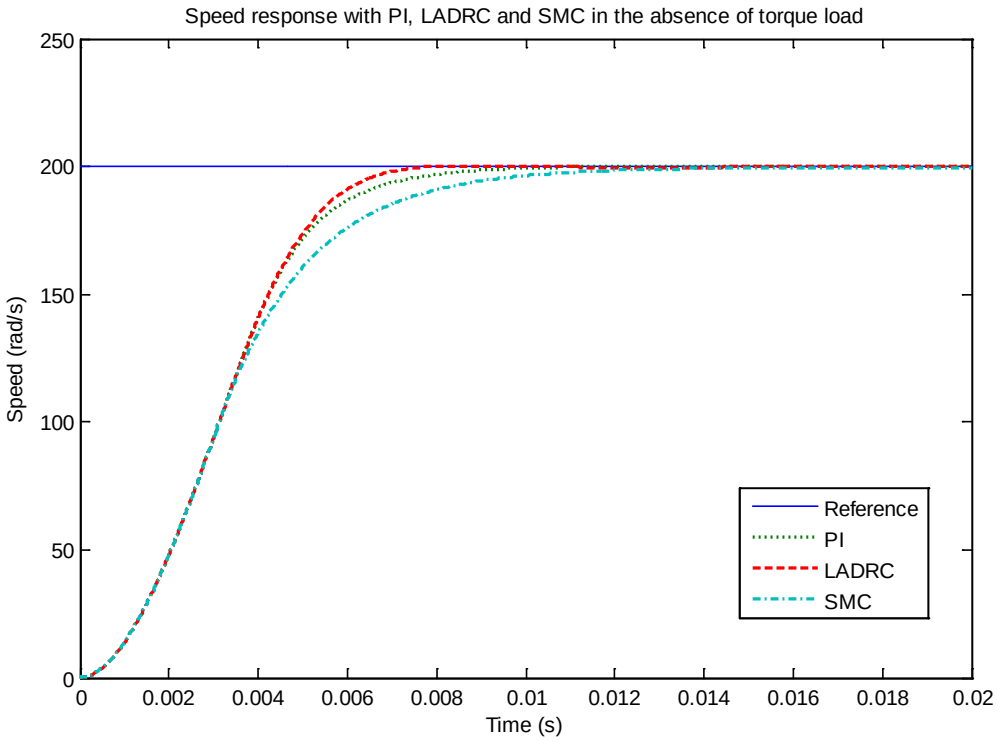

Figure 5.17: Speed responses with PI controller, LADRC and SMC in the absence of torque load

From Figure 5.17, we can see that there is no overshoot in the speed responses of PMSM speed system with PI controller, LADRC and SMC. The speed response with LADRC has the shortest settling time.

We compare the robustness of PI, LADRC and SMC against step torque load disturbance in one figure, which is shown in Figure 5.18.

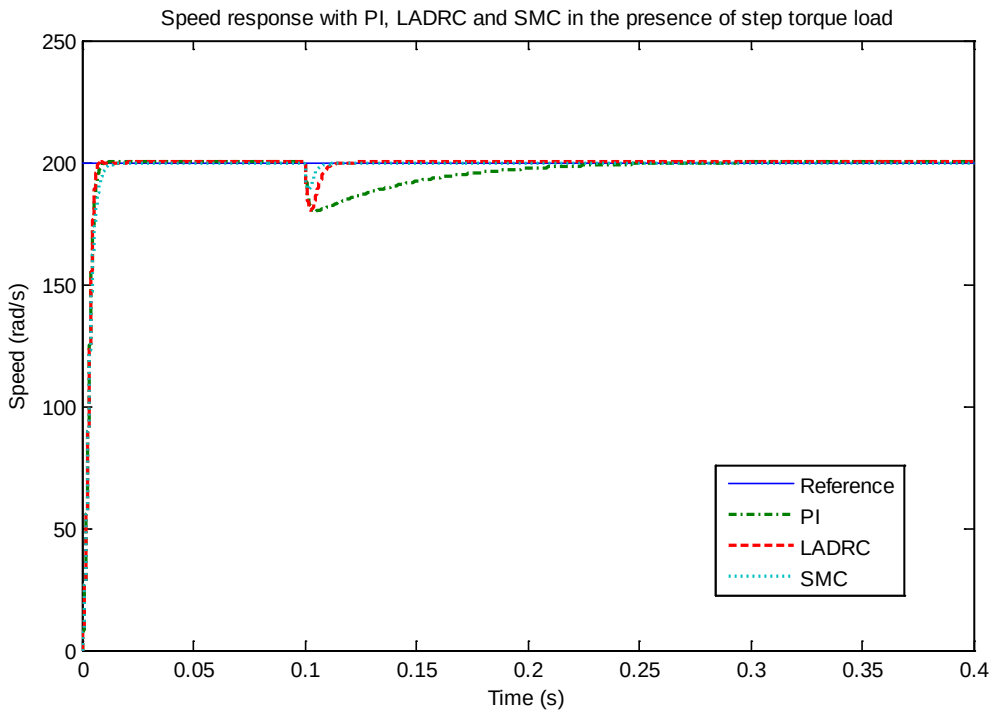

Figure 5.18: Speed responses with PI controller, LADRC and SMC in the presence of step torque load

From Figure 5.18, we can see that PI controller, LADRC and SMC can drive the speed output back to the set-point after the step torque load is applied to the system. The speed drop with SMC is smallest.

5.3 Comparison

From Figure 5.3, Figure 5.7, Figure 5.14 and Figure 5.17, we can see that the settling time of PMSM speed system with different controllers (PI controller, SMC and LADRC) is very close. And there is no overshoot. So the responses of PMSM speed system with these three controllers in the absence of torque load are all acceptable.

From Figure 5.4 and Figure 5.15, we can see that the speed drop of PMSM speed system with PI and LADRC is the almost the same, while it takes LADRC much less time to drive the speed back to the set-point.

From Figure 5.9 and Figure 5.15, we can see that it takes almost the same time for SMC and LADRC to drive the speed back to the set-point after the step torque load is applied. But the speed drop of a PMSM speed system with SMC is half the speed drop of system with LADRC. However, the control signal of SMC is more aggressive than LADRC.

From Figure 5.5, Figure 5.11 and Figure 5.16, we can see that SMC is insensitive to this parameter variation in PMSM speed system. The transit responses of PI and LADRC are degraded by this parameter variation.

5.4 Summary

The simulation results of a PMSM speed system with PI controller, SMC and LADRC using Matlab/Simulink are presented in this chapter. The comparison study of PI controller, SMC and LADRC on PMSM speed system form the aspects of dynamic performance, robustness against disturbance and parameter variations are presented.

CHAPTER VI

CONCLUSIONS AND FUTURE WORK

6.1 Conclusions

PMSM speed system with PI controller has fast transit response and stable steady state response. But the robustness of the PI controller against disturbance and parameter variations are limited. PI controller is a good option for the PMSM speed systems that do not have significant disturbance or parameter variations. The output signal of PI controller can remain at a relatively low level for PMSM speed system, which is an advantage for its real-world application.

PMSM speed system with SMC also has fast transit response and stable steady state response. In addition, SMC is robust against disturbance and parameter variations for PMSM speed system. But the good performance of PMSM speed system with SMC is at the cost of aggressive control signal. And the aggressive control signal of SMC may wear down the system in a long run. So SMC is a good option for the PMSM speed

systems that demand strong disturbance rejection capacity and robustness against parameter variations.

PMSM speed system with LADRC has desirable transit and steady state responses. The output signal of LADRC in both transit response and steady state response for PMSM speed system is quite low. LADRC has good disturbance rejection capacity when torque load disturbance is applied. But the transit response of PMSM speed system is degraded when the moment of inertia of the system is suddenly changed. LADRC is a good option for the PMSM speed system in that encounter great load variations.

6.2 Future Work

The modeling of sensors and actuators and their time lags for PMSM speed system will be researched.

The SMC with moderate control output will be studied for PMSM speed system.

The ADRC that is robustness against parameter variations without complicating the control algorithm will be investigated for PMSM speed system.

REFERENCES

1. R.Y. Tang, *Modern Permanent Magnet Machines – Theory and Design*, Beijing: China Machine Press, 1997. (In Chinese)

2. Z.M. Li, W.G. Liu, J.L. Liu, M.F. Kou and H.Z. Chen, *Rare Earth Permanent Magnet Electrical Machines*, Beijing: National Defense Industry Press, 1999. (In Chinese)

3. J.F. Gieras and M.Wing, *Permanent Magnet Motor Technology: Design and Applications*, NY: Marcel Dekker, Inc., 2002.

4. J.P. Wen, "Fractional order nonlinear feedback controller design for PMSM drives," *Hindawi Publishing Corporation, Mathematical Problems in Engineering*, vol. 2013, pp. 1-5, Mar., 2013.

5. Y.X. Su, C.H. Zheng, and B.Y. Duan, "Automatic disturbances rejection controller for precise motion control of permanent-magnet synchronous motors," *IEEE Transactions on Industrial Electronics*, vol. 52, no. 3, pp. 814–823, June, 2005.

6. Y.Z. Zhang, J.X. Song, S.H. Song and M.Y Yan, "Adaptive PID speed controller based on RBF for permanent magnet synchronous motor system," *International Conference on Intelligent Computation Technology and Automation*, vol. 1, pp. 425-428, Changsha, China, May 11-12, 2010.

7. O. Benjak and D. Gerling, "Review of position estimation methods for IPMSM drives without a position sensor part I: nonadaptive methods," *XIX International Conference on Electrical Machines*, pp. 1-6, Rome, Italy, Sep. 6-8, 2010.

8. M.S. Merzoug, and F. Nacer, "Comparison of field-oriented control and direct torque control for permanent magnet synchronous motor (PMSM)," *World Academy of Science: Engineering and Technology*, vol. 21, no. 54, pp. 299-304, Nov., 2008.

9. M. Stulrajter , V. Hrabovcova and M. Franko "Permanent magnets synchronous motor control theory," *Journal of Electrical Engineering*, vol. 58, no. 2, pp.79–84, 2007.

10. M.T. Wishart, G. Diana and R.G. Harley, “Controller design for applying field-oriented control to the permanent magnet synchronous machine,” *Electric Power Systems Research*, vol. 19, pp. 219-227, Oct.,1990.

11. D. Casadei, F. Profumo, G. Serra and A. Tani, “FOC and DTC: two viable schemes for induction motors torque control,” *IEEE Transactions on Power Electronics*, vol. 17, no. 5, Sep., 2002.

12. S.V. Paturca, M. Covrig, L. Melcescu, “Direct torque control of permanent magnet synchronous motor (PMSM) - an approach by using space vector modulation (SVM),” in Proceedings of *The 6th WSEAS/IASME Int. Conf. on Electric Power Systems, High Voltages, Electric Machines*, pp. 111-116, Tenerife, Spain, Dec. 16-18, 2006.

13. I. Takahashi and T. Noguchi, “A new quick-response and high efficiency control strategy of an induction machine,” *IEEE Transactions on Industry Applications*, vol. IA-22, pp. 820-827, Sep., 1986.

14. Y.W. Hu, C. Tian, Z.Q. You, L.X. Tang and M.F. Rahman, “Direct torque control system and sensorless technique of permanent magnet synchronous motor,” *Chinese Journal of Aeronautics*, vol. 16, no. 2, pp. 97-102, May, 2003.

15. C.Chen, S.H. Li and Y. Tian, “Active disturbance rejection control of PMSM speed-adjusting system,” *Electric Drive*, vol. 35, no. 9, 2005. (In Chinese)

16. Z. Hashemi, M. Mardaneh, M.S. Sadeghi, “High performance controller for interior permanent magnet synchronous motor drive using artificial intelligence methods,” *Scientia Iranica*, vol. 19, pp. 1788-1793, Dec., 2012.

17. K.J. Astrom and T.Hagglund, “The future of PID control,” *Control Engineering Practice*, vol. 9, pp. 1163-1175, Nov. 2001.

18. J.Q. Han, “From PID to active disturbance rejection control,” *IEEE Transactions on Industrial Electronics*, vol. 56, no. 3, pp. 900-906, Mar., 2009.

19. K. Chikh, M. Khafallah and A. Saad, “Improved DTC algorithms for reducing torque and flux ripples of PMSM based on fuzzy logic and PWM techniques,” in *Matlab - A Fundamental Tool For Scientific Computing and Engineering Applications - Volume 1*, V. Katsikis, Ed, Rijeka, Croatia: InTech, Sep., 2012, pp. 167-194.

20. J.H. Pujar and S.F. Kodad, "Digital simulation of direct torque fuzzy control of PMSM servo system," *International Journal of Recent Trends in Engineering*, vol. 2, no. 2, pp. 89-93, Nov., 2009.

21. N.J. Patil, R.H. Chile and L.M. Waghmare, "Fuzzy adaptive controllers for speed control of PMSM drive," *International Journal of Computer Applications*, vol. 1, no. 11, pp. 84-91, 2010.

22. J.M. Lazi, Z. Ibrahim, M. Sulaiman, F. A. Patakor, S.N.M. Isa, "Fuzzy logic speed controller with reduced rule base for dual PMSM drives," *World Academy of Science, Engineering and Technology*, vol. 53, no, 46, pp. 252-257, 2011

23. B. Shikkewal and V. Nandanwar, "Fuzzy logic controller for PMSM;" *International Journal of Electrical and Electronics Engineering*, vol. 1, pp. 73-78 2012.

24. B. Singh, C.L.P. Swamy, B.P. Singh, A. Chandra and K. Al-Haddad, "Performance analysis of fuzzy logic controlled permanent magnet synchronous motor drive," in Proceedings of *The 1995 IEEE IECON 21st International Conference on Industrial Electronics, Control, and Instrumentation*, vol. 1, pp. 399-405, Nov., 1995.

25. Y. Wu, H. Jiang, M. Zou, "The research on fuzzy PID control of the permanent magnet linear synchronous motor," *Physics Procedia*, vol. 24, pp. 1311-1318, 2012.

26. M. Tarnik and J. Mrugas, "Model reference adaptive control of permanent magnet synchronous motor," *Journal of Electrical Engineering*, vol. 62, no. 3, pp. 117-125, 2011.

27. Y. Luo, Y.Q. Chen and Y.G. Pi, "Authentic simulation studies of periodic adaptive learning compensation of cogging effect in PMSM position servo system," in Proceedings of *The Chinese Conference on Decision and Control*, pp. 4760-4765, Yantai, Shandong, China, July 2-4, 2008.

28. Y. Luo, Y.Q. Chen and Y.G. Pi, "Cogging effect minimization in PMSM position servo system using dual high-order periodic adaptive learning compensation," *ISA Transactions*, vol. 49, pp. 479-488, Oct. 2010.

29. S. Maier, J. Bals and M. Bodson, "Periodic disturbance rejection of a PMSM with adaptive control algorithms," *Electric Machines & Drives Conference (IEMDC), IEEE International*, pp. 1070-1075, Niagara Falls, ON, Canada , May 15-18, 2011.

30. M.J. Liu, Z.Q. Cai, X.M. Cheng and M.G. Ouyang, "Adaptive position servo control of permanent magnet synchronous motor," in Proceeding of *The American Control Conference*, vol. 1, pp. 84-89, Boston, MA, USA, June 30-July 2, 2004.

31. Y.A.R.I. Mohamed, "Adaptive self-tuning speed control for permanent-magnet synchronous motor drive with dead time," *IEEE Transactions on Energy Conversion*, vol. 21, no. 4, pp. 855-862, Dec. 2006.

32. J.H. Hung, W.B. Gao and J.C. Huang, "Variable structure control: a survey," *IEEE Transactions on Industrial Electronics*, vol. 40, no. 1, pp. 2-22, Feb. 1993.

33. J.K. Liu, *MATLAB Simulation for Sliding Mode Control*, first edition, Beijing: TsingHua University Press, Dec. 2005. (In Chinese)

34. V.I. Utkin, "Variable structure systems with sliding modes," *IEEE Transaction on Automatic Control*, vol. 22, pp. 212-222, 1977.

35. S. Vaez-Zadeh and S.M. Bakhtvar, "Cascade sliding mode control of permanent magnet synchronous motors," *IEEE 28th Annual Conference of the Industrial Electronics Society*, vol. 3, pp. 2051-2056, Sevilla, Spain Nov. 5-8, 2002.

36. J. Vittek, S.J. Dodds, P. Bris, M. Stulrajter and P. Makys, "Experimental verification of chattering free sliding mode control of the drive position employing PMSM," *Journal of Electrical Engineering*, vol. 59, no. 3, pp. 139-145, 2008.

37. C.F.J. Kuo, C.H. Hsu and C.C. Tsai, "Control of a permanent magnet synchronous motor with a fuzzy sliding-mode controller," *The International Journal of Advanced Manufacturing Technology*, vol. 32, pp. 757-763, Apr., 2007.

38. Y. Li, J.B. Son and J.M. Lee, "PMSM speed controller using switching algorithm of PD and sliding mode control," *ICROS-SICE International Joint Conference*, pp. 1260-1266, Fukuoka, Japan, Aug. 18-21, 2009.

39. M. Reichhartinger and M. Horn, “Sliding-mode control of a permanent-magnet synchronous motor with uncertainty estimation,” *World Academy of Science, Engineering and technology*, vol. 47, no. 91, pp. 511-514, 2010.

40. A. J. Koshkouei, A. S. I. Zinober and K. J. Burnham, “Adaptive sliding mode backstepping control of nonlinear systems with unmatched uncertainty,” *Asian Journal of Control*, vol. 6, no. 4, pp. 447-453, Dec., 2004.

41. A. A. Hassan, A. M. El-Sawy, Y. S. Mohamed, E. G. Shehata, “Sensorless sliding mode torque control of an IPMSM drive based on active flux concept,” Alexandria Engineering Journal, vol. 51, pp. 1-9, Mar., 2012.

42. B. F. Lv and G. X. Zhang, “Simulation and research of control-system for PMSM based on sliding mode control,” *Physics Procedia*, vol. 33, pp. 1280-1285, 2012.

43. Y. J. Guo and H. Long, “Self organizing fuzzy sliding mode controller for the position control of a permanent magnet synchronous motor drive,” *Ain Shams Engineering Journal*, vol. 2, pp. 109-118, 2011.

44. S. Brock, “Sliding mode control of a permanent magnet direct drive under non-linear friction,” *The International Journal for Computation and Mathematics in Electrical and Electronic Engineering*, vol. 30, pp.853-863, 2011.

45. V. I. Utkin, “Sliding mode control: mathematical tools, design and applications,” in *Nonlinear and Optimal Control Theory*, *Lecture Notes in Mathematics*, vol. 1932, P. Nistri and G. Stefani, Ed, Berlin, Germany: Springer Berlin Heidelberg, 2008, pp 289-347.

46. J. Q. Han, “Auto disturbances rejection controller and its applications,” *Control and Decision*, vol. 13, no. 1, pp. 19-23, Jan., 1998. (In Chinese)

47. J. Q. Han and W. Wang, “Nonlinear tracking-differentiator,” *Syst. Sci. and Math*., vol. 14, no. 2, pp. 177-183, 1994. (In Chinese)

48. J. Q. Han, “Nonlinear state error feedback control law - NLSEF,” *Control and Decision*, vol. 10, no. 3, pp. 177-183, May, 1995. (In Chinese)

49. J. Q. Han, “Extended state observer for a class of uncertain plants,” *Control and Decision*, vol. 10, no. 1, pp. 85–88, 1995. (In Chinese)

50. Z. Q. Gao, Y. Huang and J. Q. Han, "An alternative paradigm for control system design," in Proceedings of *The 40th IEEE Conference on Decision and Control*, vol.5, pp. 4578-4585, 2001.

51. Z. Q. Gao, "Scaling and bandwidth-parameterization based controller tuning," in Proceedings of *The American control conference*, vol. 6, pp. 4989-4996, Denver, CO, USA, June 4-6, 2003.

52. S. H. Li, H. X. Liu and S. H. Ding, "A speed control for a PMSM using finite-time feedback control and disturbance compensation," *Transactions of The Institute of Measurement and Control*, vol. 32, pp. 170-187, 2010.

53. S. H Li, C. J. Xia and X. Zhou, "Disturbance rejection control method for permanent magnet synchronous motor speed-regulation system," *Mechatronics*, vol. 22, pp. 706-714, Sep., 2012.

54. Y. Tang, J. J. H. Paulides, E. Kazmin and E. A. Lomonova, "Investigation of winding topologies for permanent magnet in-wheel motors," *The International Journal for Computation and Mathematics in Electrical and Electronic Engineering*, vol. 31 no. 1, pp. 88-107, 2012.

55. N. K. De and S. K. Dutta, *Electric Machines and Electric Drives: Problems with Solutions*, New Delhi, India: PHI Learning Private Limited, Jan., 2012.

56. P. Pillay, and R. Krishnan, "Modeling of permanent magnet motor drives," *IEEE Transactions on Industrial Electronics*, vol. 35, no.4, pp. 537-541, Nov., 1988.

57. R. Krishnan, *Permanent Magnet Synchronous and Brushless DC Motor Drives*, Boca Raton, FL: CRC Press, 2010.

58. J. J. E. Slotine and W. P. Li, *Applied nonlinear control*, Prentice-Hall, 1991.

59. Z. Q. Gao, S. H. Hu, and F. J. Jiang, "A novel motion control design approach based on active disturbance rejection," *Decision and control, Proceedings of the 40th IEEE conference*, vol. 5, pp. 4877-4882, 2001.

60. Z. G. Wang, J. X. Jin, Y. G. Guo and Y. D. Zhan, "Modeling and simulation of PMSM control system based on SVPWM," *The 27th Chinese Control Conference*, pp. 724 – 728, 2008.